methrin, metribuzine, kelthane, pentachlorophenol, dicyclohexyl phthalate, diethylhexyl phthalate, and bisphenol A produced a significant decrease in activity ($P < 0.01$). Moreover, in agreement with a previous study of ours (7), tributyltin inhibited aromatase activity in this cell line. As the effect of benomyl was most remarkable, in this study we focused on the mechanism underlying benomyl stimulation of aromatase activity. Importantly, 10^{-5} M benomyl also caused a 2-fold increase in aromatase activity in cultured human granulosa cells obtained from a woman who underwent *in vitro* fertilization (Fig. 1B), indicating that the effect of benomyl on aromatase activity is not a cell line-specific effect. The stimulatory effect of benomyl on aromatase activity exhibited a dose-dependent relationship for concentrations ranging from 10^{-6} –10^{-5} M (Fig. 2A). The effect of 10^{-5} M benomyl also exhibited a time dependence for at least the 80-h incubation tested here (Fig. 2B).

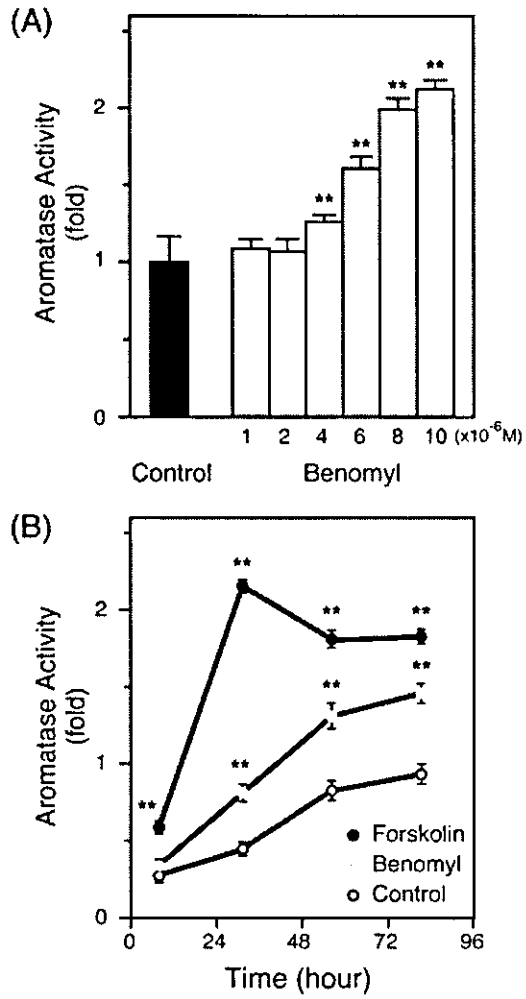

FIG. 2. Effect of benomyl on aromatase activity in cultured KGN cells. A, KGN cells were cultured in the presence or absence of 10^{-6}–10^{-5} M benomyl for 24 h (dose dependency). B, KGN cells were cultured in the presence of 10^{-5} M benomyl for 24–96 h (time dependency). Aromatase activity was assayed as described in *Materials and Methods*. Each value indicates the mean ± SD of three experiments, with triplicate plates per point. *, $P < 0.05$; **, $P < 0.01$ (*vs.* control).

Effect of benomyl on transcription of CYP19

To investigate whether these effects of benomyl were regulated at the level of transcription, we determined the levels of aromatase mRNA expression by both RT-PCR and quantitative real-time PCR. The KGN cells were incubated with 10^{-7} M forskolin, 500 mIU/ml human menopausal gonadotropin (hMG), 10^{-5} M benomyl, or DMSO (control) and total RNA was extracted. We amplified both *CYP19* and β-actin mRNA (used as an internal control to normalize the levels of *CYP19* expression). Both forskolin and hMG, which are known to activate the cAMP-protein kinase A (PKA) pathway, stimulated the expression of aromatase mRNA. Similarly, benomyl increased aromatase mRNA levels relative to β-actin (Fig. 3A). This was further confirmed using real-time PCR methods. Namely, 10^{-5} M benomyl caused a 3.47-fold increase in aromatase mRNA compared with the treatment with DMSO (control; Table 1). We next analyzed the effects of these compounds on transcription of the *CYP19* promoter. KGN cells were transfected with the pGL3-basic luciferase reporter plasmid that contains 4 kb of aromatase promoter II. Forskolin, benomyl, or DMSO (control) were then added and incubated for 24 h. As shown in Fig. 3B, benomyl significantly stimulated luciferase activity. All these data clearly indicate that benomyl predominantly up-regulates aromatase activity through the transcription of *CYP19*.

Effects of benomyl on cAMP production and CRE-mediated transcription

It is well known that the expression of *CYP19* in ovarian granulosa cells is mainly regulated by the cAMP-PKA pathway (3, 4, 22–24), resulting in an adenylate cyclase-mediated rise in cAMP levels and activation of PKA. We thus examined whether the stimulatory effect of benomyl on aromatase activity is mediated by this system. For this analysis, KGN cells were treated with 10^{-7} M forskolin, 500 mIU/ml hMG, 10^{-5} M benomyl, or DMSO (control). To prevent the metabolic effect of phosphodiesterase on cAMP, 0.5 mM 3-isobutyl-1-methylxanthine (a specific inhibitor of phosphodiesterase activity) was added to the culture medium. The concentration of cAMP in the culture medium was measured after 48 h. As shown in Fig. 4A, forskolin and hMG increased cAMP levels, whereas benomyl did not. We further analyzed the effect of benomyl on CRE-mediated transcription using a reporter plasmid containing two copies of the CRE sequence. As shown in Fig. 4B, both forskolin, a known activator of adenylate cyclase, and hMG stimulated CRE-mediated activity, whereas benomyl had no effect. These results strongly suggest that the cAMP-PKA pathway is unlikely to be the main mechanism that mediates the benomyl-mediated increase in aromatase activity.

Several kinases other than PKA are activated by FSH receptors, including protein kinase B (PKB)/Akt, serum and glucocorticoid-induced kinase (Sgk), ERK, and p38 MAPK, protein tyrosine kinase also stimulates FSH signal

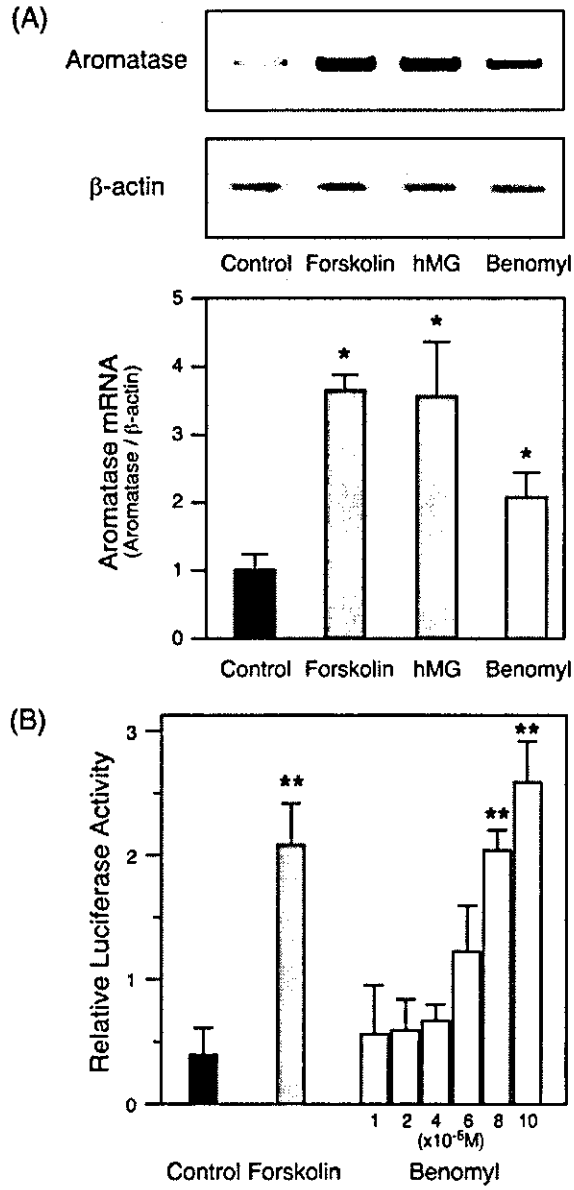

FIG. 3. Effect of benomyl on the expression of aromatase mRNA in cultured KGN cells. A, KGN cells were cultured in the presence or absence of 10^{-7} M forskolin, 500 mIU/ml hMG, or 10^{-5} M benomyl for 24 h. Total RNA was then extracted, and semiquantitative RT-PCR was performed as described in *Materials and Methods*. Images of agarose gel electrophoresis of RT-PCR products are indicated. The relative amount of cytochrome P450 aromatase to β-actin mRNA was determined from the intensity of the ethidium bromide. B, KGN cells were cultured in the presence or absence of 10^{-7} M forskolin, 500 mIU/ml hMG, or 10^{-6}–10^{-5} M benomyl for 24 h, andthe relative luciferase activity of the *CYP19* gene was measured as described in *Materials and Methods*. Each value indicates the mean ± SD of three experiments, with triplicate plates per point. *, $P < 0.05$; **, $P < 0.01$ (*vs.* control).

(25–28). Using a variety of kinase inhibitors, the effect of benomyl on kinases other than PKA was examined. The increased aromatase activity by benomyl was not significantly blocked by kinase inhibitors for PKB/Akt and Sgk (0.1–10 μM wortmannin), ERK (10 μM U0126 or 10 μM PD98059), protein tyrosine kinase (10 μM genistein, 50 μM AG490, and 100 nM AG1478), which suggests that these kinases do not mediate the effects of benomyl.

Effect of benomyl on the production of progesterone, P450scc mRNA, and StAR mRNA

We have previously shown that KGN cells mainly express StAR and P450scc, rather than aromatase (13). We measured the levels of progesterone after incubation with 10^{-7} M forskolin, 500 mIU/ml hMG, 10^{-5} M benomyl, or DMSO (control). Progesterone levels in the medium were significantly increased by forskolin and hMG (Fig. 5A). Benomyl, however, did not alter basal progesterone production. Additionally, we determined whether benomyl affected the expression of mRNA for these steroidogenesis-related proteins and enzymes. The KGN cells were incubated with 10^{-7} M forskolin, 500 mIU/ml hMG, 10^{-5} M benomyl, or DMSO (control), and the total RNA was extracted. We then determined the levels of P450scc and StAR mRNA by both RT-PCR and quantitative real-time PCR. As shown in Fig. 5B and Table 1, benomyl did not affect the mRNA expression levels of P450scc and StAR relative to β-actin or glyceraldehyde-3-phosphate dehydrogenase. Together these results indicate the effect of benomyl on steroidogenesis in KGN cells is specific to aromatase.

Effect of the benomyl metabolite, carbendazim, on aromatase expression

It is well established that in either aqueous solutions or soil, benomyl rapidly degrades to its breakdown product carbendazim (Fig. 6A) (15, 16). We therefore investigated the effect of carbendazim on aromatase expression. As expected, like benomyl, 10^{-5} M carbendazim significantly induced transcription of *CYP19* (Fig. 6B). We also determined aromatase expression levels by Western blotting. Benomyl and carbendazim increased the expression of aromatase almost equally, although the effect was weaker than that of 10^{-7} M forskolin or 500 mIU/ml hMG (Fig. 6C), which is consistent with the results of the luciferase assay (Fig. 6A). Carbendazim (10^{-5} M) increased aromatase activity to a level similar to that observed with 10^{-5} M benomyl. These results suggest that the effect of benomyl on aromatase is mediated by carbendazim.

Effect of taxol on benomyl-stimulated aromatase activity

Microtubules are ubiquitous components of cytoskeletons that contribute to the translocation of cellular organelles and secretory materials. A dynamic equilibrium exists between dimeric tubulin and microtubules, with net assembly and disassembly occurring at opposite ends of each complex, and is thought to be closely associated with the function of the cytoskeleton. Benomyl is known to interfere with the assembly of microtubules (14), whereas taxol is a potent promoter of microtubule assembly and is thought to stabilize the polymerized form of tubulin *in vitro* (29, 30). We thus compared the effect of benomyl on aromatase activity with that of taxol. As shown in Fig. 7A, treatment with 10^{-5} M benomyl or 10^{-9} M taxol caused clear changes in KGN cell morphology.

TABLE 1. Relative quantitation of mRNA expressions of aromatase, StAR, and P450scc determined by quantitative real-time PCR

Treatment	Target	Average C_T	GAPDH average C_T	ΔC_T	$\Delta\Delta C_T$	Ratio (relative to control)
Control	Aromatase	28.12 ± 0.30		11.60 ± 0.74	0.00 ± 0.74	1.00 (0.60–1.67)
	P450scc	27.03 ± 0.13	16.52 ± 0.45	10.51 ± 0.34	0.00 ± 0.34	1.00 (0.79–1.26)
	StAR	26.89 ± 0.41		10.37 ± 0.20	0.00 ± 0.20	1.00 (0.87–1.15)
Benomyl	Aromatase	26.84 ± 0.42		9.80 ± 0.15	1.80 ± 0.15	3.47 (3.13–3.86)
	P450scc	27.11 ± 0.09	17.03 ± 0.29	10.07 ± 0.36	0.44 ± 0.36	1.35 (1.06–1.73)
	StAR	26.81 ± 0.22		9.77 ± 0.07	0.59 ± 0.48	1.51 (1.08–2.11)

KGN cells were cultured in the presence or absence of 10^{-5} M benomyl. After 24 h of culture, total RNA was extracted and quantitative real-time PCR was performed as described in *Materials and Methods*. Relative mRNA expression was normalized to that of DMSO (control)-treated cells using the established equation. $2^{-\Delta\Delta CT}$, Where C_T is the cycle number at the chosen amplification threshold; ΔC_T = C_T target (aromatase, P450scc, or StAR) − C_T GAPDH (reference) and $\Delta\Delta C_T$ = ΔC_T benomyl-ΔC_T control.

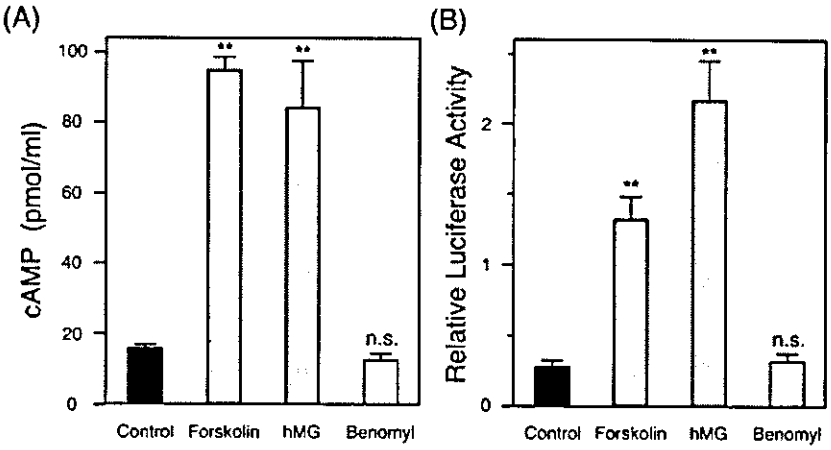

FIG. 4. Effect of benomyl on cAMP production and CRE-mediated transcription in cultured KGN cells. A, KGN cells were cultured in the presence or absence of 10^{-7} M forskolin, 500 mIU/ml hMG, or 10^{-5} M benomyl for 48 h. The cAMP concentration in the medium was then measured. B, KGN cells were cultured in the presence or absence of 10^{-7} M forskolin, 500 mIU/ml hMG, or 10^{-5} M benomyl for 24 h, and CRE-mediated transcription was measured by the relative luciferase activity of the pGL3-Basic luciferase reporter plasmid containing two copies of CRE. Each value indicates the mean ± SD of three experiments, with triplicate plates per point. *, $P < 0.05$; **, $P < 0.01$ (*vs.* control).

Namely, KGN cells treated with benomyl or taxol became rounder than those incubated with DMSO (control) or 10^{-7} M forskolin. In addition, immunofluorescence staining with anti-α-tubulin revealed that taxol caused dense staining of bundles in the perinuclear region. These responses by the cells treated with taxol have been previously reported in various cell types, including ovarian granulosa cells (30, 31). Benomyl caused a similar change in cell shape and in the subcellular bundle pattern. Although we could not refer to fine structural changes in the bundles, it was evident that both treatments clearly produced a different pattern compared with the control or forskolin. Additionally, we investigated the effect of taxol on aromatase promoter II. Taxol increased aromatase-luciferase activity to the same extent as benomyl (Fig. 7B). Taxol also increased aromatase activity to similar levels as benomyl (data not shown). These results suggest that disruption of the dynamic equilibrium between dimeric tubulin and microtubules by microtubule-interfering agents (MIAs) may lead to increased aromatase activity.

Discussion

In the present study the screening of 55 potential chemicals as endocrine disruptors found that only benomyl stimulated aromatase activity in cultured human granulosa cell line or KGN cells. The stimulatory effect of benomyl on aromatase activity was associated with comparable changes in aromatase mRNA levels. In addition, the luciferase activity of aromatase promoter II (4 kb) in transfected KGN cells was increased with the addition of benomyl. Based on these findings, the benomyl-induced increase in aromatase activity appears to be mainly regulated by the transcription of *CYP19*. Importantly, the rapidly produced metabolite of benomyl, carbendazim (15–17), was equally effective in stimulating aromatase activity. Thus, the effect of benomyl could be mediated by carbendazim, rather than benomyl itself, as suggested in benomyl-induced testicular toxicity (32).

The stimulatory effect of the benzimidazole fungicide, benomyl, on aromatase activity is somewhat surprising because some imidazoles, such as fadrozole and vordozole, suppress aromatase activity and act as potent aromatase inhibitors through the formation of tightly associated aromatase-inhibitor complexes that disturb heme binding and substrate binding of aromatase (33). Thus, benomyl is considered to be a unique type of imidazole because it stimulates aromatase activity.

FSH is the major physiological stimulator of human *CYP19* expression, by increasing cAMP levels. This mechanism is mediated by the CRE, which binds the *trans*-acting factors of the CRE-binding protein/activating transcription factor family (22, 34). However, it is unlikely that this cAMP-PKA pathway mediates the stimulatory effect of benomyl on *CYP19* expression, because benomyl did not increase either cAMP levels or CRE-mediated transcriptional activity. In addition, several other kinases, including PKB/Akt, Sgk, ERK, and protein tyrosine kinase, which are reported to be activated by FSH signal (25–28), seemed to be unrelated to this mechanism, based on the effect of inhibitors for these kinases.

Cellular cytoskeletons consist of an integrated network of microtubules, microfilaments, and intermediate filaments, in

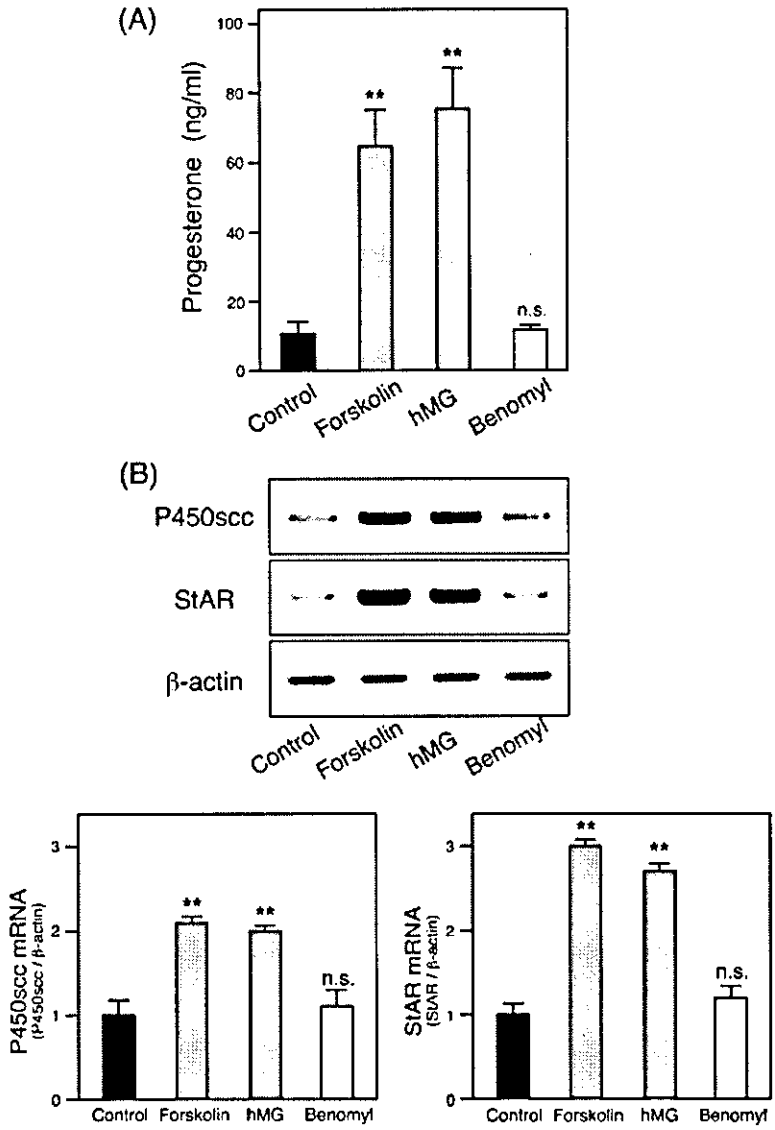

FIG. 5. Effect of benomyl on the production of progesterone (A) and expressions of P450scc and StAR mRNA in cultured KGN cells (B). A, KGN cells were cultured in the presence or absence of 10^{-7} M forskolin, 500 mIU/ml hMG, or 10^{-5} M benomyl for 24 h. The progesterone concentration in the medium was then measured by specific RIA. B, KGN cells were cultured in the presence or absence of 10^{-7} M forskolin, 500 mIU/ml hMG, or 10^{-5} M benomyl for 24 h, and the expressions of P450scc, StAR, and β-actin mRNA were determined by RT-PCR. Each value indicates the mean ± SD of three experiments, with triplicate plates per point. *, $P < 0.05$; **, $P < 0.01$ (*vs.* control).

which changes in the distribution of one component can profoundly influence that of another. It can thus be imagined that steroidogenesis involves controlled organization of microtubules, which may facilitate the movement of substrates into organelles such as mitochondria or microsomes, possibly by bringing these cellular inclusions closer together. This role of microtubules in regulating ovarian granulosa cell steroidogenesis has been previously demonstrated (35–40). For example, colchicine and nocodazole, two agents that depolymerize microtubules, significantly stimulate progesterone production in antral stage granulosa cells of Sprague-Dawley rats, whereas taxol, a stabilizing agent of microtubules, markedly reduced FSH-stimulated production of progesterone in both preantral and antral cells (35). In our study, both benomyl, a depolymerizing agent of microtubules, and taxol, a stabilizing agent of microtubules, had similar effects on the stimulation of aromatase activity in KGN cells. The effect of benomyl or taxol was accompanied by characteristic changes in cell shape and subcellular reorganization of microtubules. Interestingly, in agreement with our results, Cameron *et al.* (40) reported that nanogram per milliliter concentrations of taxol increase estrogen production in three ovarian cancer cell lines and in JEG-3 choriocarcinoma cells as well as immunostaining for aromatase in cancer cells. These results strongly suggest that deregulation of the dynamic equilibrium of microtubule assembly/disassembly caused by MIA may play an important role in increasing aromatase activity in KGN cells.

It is also noteworthy that the effect of benomyl in steroidogenesis was specifically observed in the microsomal enzyme, aromatase, but was not evident in the mitochondrial protein, StAR, or in the enzyme P450scc. When it reorganizes the intracellular distribution and spacing toward microsomes and mitochondria, benomyl may influence the cross-bridges linking microtubules and organelles. These differences may be simply dependent on the MIA type used or the

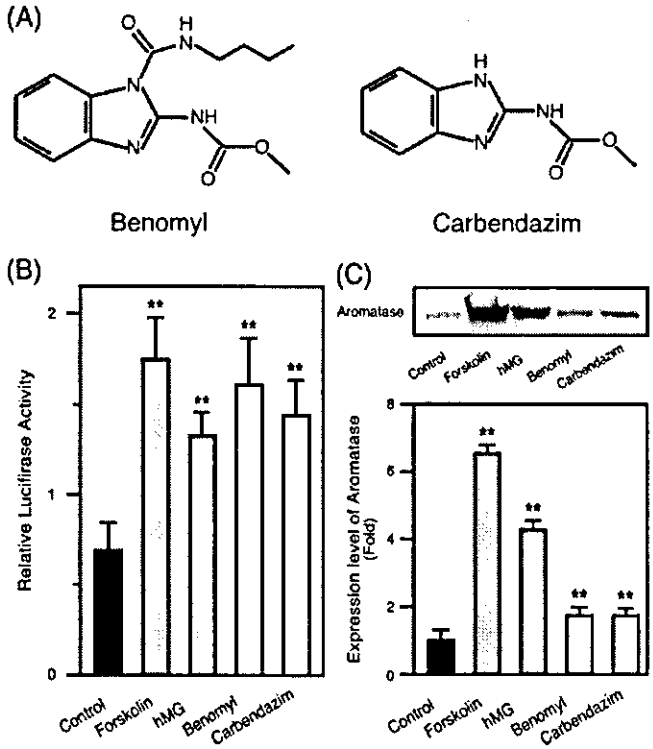

FIG. 6. Effect of the benomyl and its metabolite, carbendazim, on transcription of the *CYP19* promoter (B) and aromatase protein expression (C). A, Chemical structure of benomyl and its metabolite, carbendazim. B, Effect of benomyl or carbendazim on the transcription of *CYP19* promoter (promoter II) in cultured KGN cells. KGN cells were cultured in the presence or absence of 10^{-7} M forskolin, 500 mIU/ml hMG, 10^{-5} M benomyl, or 10^{-5} M carbendazim for 24 h, and the relative luciferase activity was measured as described in *Materials and Methods*. C, Effect of benomyl or carbendazim on aromatase expression in cultured KGN cells. KGN cells were cultured in the presence or absence of 10^{-7} M forskolin, 500 mIU/ml hMG, 10^{-5} M benomyl, or 10^{-5} M carbendazim for 24 h, and the expression of aromatase was examined by Western blot analysis using antibodies for aromatase. Thirty micrograms of protein were loaded into each lane. Each value indicates the mean ± SD of three experiments, with triplicate plates per point. *, $P < 0.05$; **, $P < 0.01$ (*vs.* control).

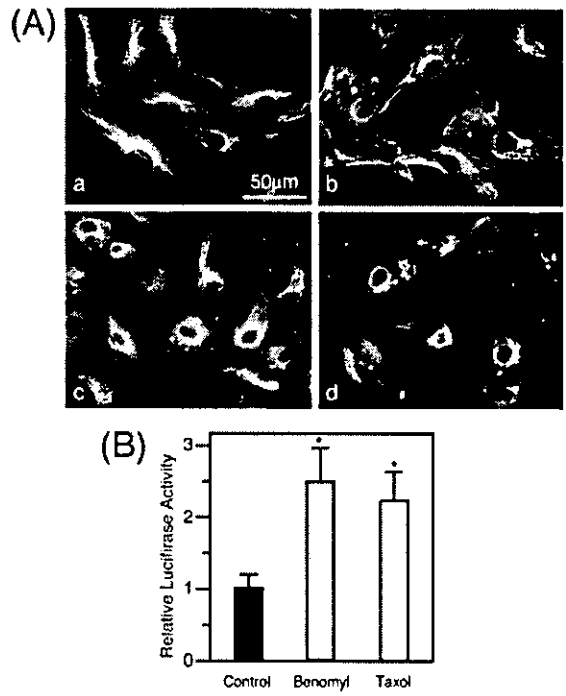

FIG. 7. Effects of MIAs on KGN cells. A, Anti-α-tubulin staining of control cells (a) and cells treated with 10^{-7} M forskolin (b), 10^{-5} M benomyl (c), and 10^{-9} M taxol (d), respectively. Immunofluorescence staining was performed as described in *Materials and Methods*. B, KGN cells were cultured in the presence or absence of 10^{-5} M benomyl or 10^{-9} M taxol for 24 h, and the relative luciferase activity of the *CYP19* gene was measured. Each value indicates the mean ± SD of three experiments, with triplicate plates per point. *, $P < 0.05$; **, $P < 0.01$ (*vs.* control).

cell type and conditions. Although little is known about the molecular mechanism of how MIA works, the partial involvement of the c-Jun N-terminal kinase signal, one subgroup of MAPK (41), has been implicated in the effects mediated by taxol. It has been reported that microtubules can anchor the transcription factors, Smads, in an inactive state in cytoplasm. Activation by a ligand or MIA results in dissociation of Smads from the microtubule network (42). Likewise, MIA may activate some transcription factors, which are essential for *CYP19* gene transcription. Further investigation is needed to determine the mechanism of MIA and benomyl-mediated stimulation of *CYP19* expression.

A logical concern based on our results would be that long-term or excessive exposure of wildlife and humans to benomyl, carbendazim, or taxol might contribute to serious estrogen-mediated pathologies, such as tumor promotion and inappropriate sexual differentiation. During critical development periods, such as embryonic perinatal and pubertal development, benomyl-mediated induction of aromatase could result in inappropriate feminization. In human females, the local production of estrogens due to the increased levels of aromatase expression in breast adipose or stromal tissue has been associated with an increased risk of breast cancer (3, 43). Interestingly, taxol inhibits TNF-α-stimulated aromatase activity in stromal fibroblasts derived from normal or malignant breast tissues, suggesting that taxol may have a therapeutic potential in the treatment of breast cancer (44). However, they observed no such effect by another class of MIA, indicating that the effect of each MIA is tissue specific and should be carefully considered in its evaluation as an endocrine disruptor chemical.

Benomyl is especially known to be toxic to the male reproductive system of rodents and dogs, producing hypospermatogenesis and multinucleated germ cells. Because benomyl or its metabolite carbendazim inhibits microtubule formation in fungi, it has been proposed by many investigators that severe testicular dysfunction may be caused by the impediment of cell division and other microtubule-dependent processes of spermatogenesis (45–49). However, it is not clear whether this occurs in human males. In addition, because the same promoter usage of *CYP19* has been identified in the ovary and testis (23, 24), it might be intriguing to examine the possibility that benomyl contributes to male feminization by affecting testicular aromatase activity.

In summary, the human granulosa cancer cell line, KGN, cell system that we have developed has proven useful in identifying a potentially essential target for endocrine disruptors in aromatase assays. Using this system, we have demonstrated for the first time that benomyl and its metabolite, carbendazim, stimulate aromatase activity independently of cAMP activation and several other kinase-related pathways. The effect of benomyl or carbendazim was regulated mainly at the level of transcription and seems to be closely related to the unbalanced assembly/disassembly organization of microtubules.

Acknowledgments

Received September 8, 2003. Accepted December 15, 2003.

Address all correspondence and requests for reprints to: Toshihiko Yanase, M.D., Department of Medicine and Bioregulatory Science (Third Department of Internal Medicine), Graduate School of Medical Sciences, Kyushu University, 3-1-1 Maidashi, Higashi-ku, Fukuoka 812-8582, Japan. E-mail: yanase@intmed3.med.kyushu-u.ac.jp.

This work was supported in part by a grant from the Ministry of Health, Labor, and Welfare of Japan.

References

1. **Colborn T, Dumanoski D, Myers JP** 1996 Our stolen future. New York: Penguin
2. **McLachlan JA** 2001 Environmental signaling: what embryos and evolution teach us about endocrine disrupting chemicals. Endocr Rev 22:319–341
3. **Simpson ER, Mahendroo MS, Means GD, Kilgore MW, Hinshelwood MM, Graham-Lorence S, Amarneh B, Ito Y, Fisher CR, Michael MD, Mendelson CR, Bulun SE** 1994 Aromatase cytochrome P450, the enzyme responsible for estrogen biosynthesis. Endocr Rev 15:342–355
4. **Bulun SE, Rosenthal IM, Brodie AM, Inkster SE, Zeller WP, DiGeorge AM, Frasier SD, Kilgore MW, Simpson ER** 1994 Use of tissue-specific promoters in the regulation of aromatase cytochrome P450 gene expression in human testicular and ovarian sex cord tumors, as well as in normal fetal and adult gonads. J Clin Endocrinol Metab 78:1616–1621
5. **Sanderson JT, Seinen W, Giesy JP, van den Berg M** 2000 2-Chloro-s-triazine herbicides induce aromatase (CYP19) activity in H295R human adrenocortical carcinoma cells: a novel mechanism for estrogenicity? Toxicol Sci 54:121–127
6. **You L, Sar M, Bartolucci E, Ploch S, Whitt M** 2001 Induction of hepatic aromatase by *p,p'*-DDE in adult male rats. Mol Cell Endocrinol 178: 207–214
7. **Saitoh M, Yanase T, Morinaga H, Tanabe M, Mu YM, Nishi Y, Nomura M, Okabe T, Goto K, Takayanagi R, Nawata H** 2001 Tributyltin or triphenyltin inhibits aromatase activity in the human granulosa-like tumor cell line KGN. Biochem Biophys Res Commun 289:198–204
8. **Vinggaard AM, Hnida C, Breinholt V, Larsen JC** 2000 Screening of selected pesticides for inhibition of CYP19 aromatase activity in vitro. Toxicol In Vitro 14:227–234
9. **Andersen HR, Andersson AM, Arnold SF, Autrup H, Barfoed M, Beresford NA, Bjerregaard P, Christiansen LB, Gissel B, Hummel R, Jorgensen EB, Korsgaard B, Le Guevel R, Leffers H, McLachlan J, Moller A, Nielsen JB, Olea N, Oles-Karasko A, Pakdel F, Pedersen KL, Perez P, Skakkebaek NE, Sonnenschein C, Soto AM, Sumpter JP, Thorpe SM, Grandjean P** 1999 Comparison of short-term estrogenicity tests for identification of hormone-disrupting chemicals. Environ Health Perspect 107(Suppl 1):89–108
10. **Andersen HR, Vinggaard AM, Rasmussen TH, Gjermandsen IM, Bonefeld-Jorgensen EC** 2002 Effects of currently used pesticides in assays for estrogenicity, androgenicity, and aromatase activity in vitro. Toxicol Appl Pharmacol 179:1–12
11. **Davis BJ, Weaver R, Gaines LJ, Heindel JJ** 1994 Mono-(2-ethylhexyl) phthalate suppresses estradiol production independent of FSH-cAMP stimulation in rat granulosa cells. Toxicol Appl Pharmacol 128:224–228
12. **Lovekamp TN, Davis BJ** 2001 Mono-(2-ethylhexyl) phthalate suppresses aromatase transcript levels and estradiol production in cultured rat granulosa cells. Toxicol Appl Pharmacol 172:217–224
13. **Nishi Y, Yanase T, Mu Y, Oba K, Ichino I, Saito M, Nomura M, Mukasa C, Okabe T, Goto K, Takayanagi R, Kashimura Y, Haji M, Nawata H** 2001 Establishment and characterization of a steroidogenic human granulosa-like tumor cell line, KGN, that expresses functional follicle-stimulating hormone receptor. Endocrinology 142:437–445
14. **Davidse LC** 1986 Benzimidazole fungicide: mechanism of action and biological impact. Annu Rev Phytopathol 24:43–65
15. **Tang SC, Yanagihara K, Zhang Y** 1992 1-Butyl-isocyanate from benlate formulation. Arch Environ Contam Toxicol 23:270–272
16. **Chiba M, Cherniak EA** 1978 Kinetic study of reversible conversion of methyl 1-(butylcarbamoyl)-2-benzimidazolecarbamate (MBC) and *n*-butyl isocyanate (BIC) in organic solvents. J Agric Food Chem 26:573–576
17. **Dalvi RR** 1992 Effect of the fungicide benomyl on xenobiotic metabolism in rats. Toxicology 71:63–68
18. **Mu YM, Yanase T, Nishi Y, Waseda N, Oda T, Tanaka A, Takayanagi R, Nawata H** 2000 Insulin sensitizer, troglitazone, directly inhibits aromatase activity in human ovarian granulosa cells. Biochem Biophys Res Commun 271: 710–713
19. **Honma M, Satoh T, Takezawa J, Ui M** 1977 An ultrasensitive method for the simultaneous determination of cyclic AMP and cyclic GMP in small-volume samples from blood and tissue. Biochem Med 18:257–273
20. **Harada N, Yamada K, Saito K, Kibe N, Dohmae S, Takagi Y** 1990 Structural characterization of the human estrogen synthetase (aromatase) gene. Biochem Biophys Res Commun 166:365–372
21. **Sasano H, Nagura H, Harada N, Goukon Y, Kimura M** 1994 Immunolocalization of aromatase and other steroidogenic enzymes in human breast disorders. Hum Pathol 25:530–535
22. **Michael MD, Kilgore MW, Morohashi K, Simpson ER** 1995 Ad4BP/SF-1 regulates cyclic AMP-induced transcription from the proximal promoter (PII) of the human aromatase P450 (CYP19) gene in the ovary. J Biol Chem 270: 13561–13566
23. **Fitzpatrick SL, Richards JS** 1994 Identification of a cyclic adenosine 3',5'-monophosphate-response element in the rat aromatase promoter that is required for transcriptional activation in rat granulosa cells and R2C leydig cells. Mol Endocrinol 8:1309–1319
24. **Young M, McPhaul MJ** 1998 A steroidogenic factor-1-binding site and cyclic adenosine 3',5'-monophosphate response element-like elements are required for the activity of the rat aromatase promoter in rat Leydig tumor cell lines. Endocrinology 139:5082–5093
25. **Richards JS** 2001 New signaling pathways for hormones and cyclic adenosine 3',5'-monophosphate action in endocrine cells. Mol Endocrinol 15: 209–218
26. **Gonzalez-Robayna IJ, Falender AE, Ochsner S, Firestone GL, Richards JS** 2000 Follicle-stimulating hormone (FSH) stimulates phosphorylation and activation of protein kinase B (PKB/Akt) and serum and glucocorticoid-lnduced kinase (Sgk): evidence for A kinase-independent signaling by FSH in granulosa cells. Mol Endocrinol 14:1283–1300
27. **Costrici N, Elberg G, Lunenfeld B, Pariente C, Dor J, Kanety H, Karasik A** 1995 A cytosolic protein tyrosine kinase activity is induced by follicle stimulating hormone and insulin like growth factor-I in human granulosa cells. Endocrinology 136:4705–4708
28. **Moore RK, Otsuka F, Shimasaki S** 2001 Role of ERK1/2 in the differential synthesis of progesterone and estradiol by granulosa cells. Biochem Biophys Res Commun 289:796–800
29. **Schiff PB, Horwitz SB** 1980 Taxol stabilizes microtubules in mouse fibroblast cells. Proc Natl Acad Sci USA 77:1561–1565
30. **Albertini DF, Clark JI** 1981 Visualization of assembled and disassembled microtubule protein by double label fluorescence microscopy. Cell Biol Int Rep 5:387–397
31. **Herman B, Langevin MA, Albertini DF** 1983 The effects of taxol on the organization of the cytoskeleton in cultured ovarian granulosa cells. Eur J Cell Biol 31:34–45
32. **Lim J, Miller MG** 1997 The role of the benomyl metabolite carbendazim in benomyl-induced testicular toxicity. Toxicol Appl Pharmacol 142: 401–410
33. **Harada N, Honda SI, Hatano O** 1999 Aromatase inhibitors and enzyme stability. Endocr Relat Cancer 6:211–218
34. **Meyer TE, Habener JF** 1993 Cyclic adenosine 3', 5'-monophosphate response element binding protein (CREB) and related transcription-activating deoxyribonucleic acid-binding proteins. Endocr Rev 14:269–290
35. **Carnegie JA, Dardick I, Tsang BK** 1987 Microtubules and the gonadotropic regulation of granulosa cell steroidogenesis. Endocrinology 120:819–828
36. **Carnegie JA, Tsang BK** 1987 Microtubules and the calcium-dependent regulation of rat granulosa cell steroidogenesis. Biol Reprod 36:1007–1015
37. **Carnegie JA, Tsang BK** 1988 The cytoskeleton and rat granulosa cell steroidogenesis: possible involvement of microtubules and microfilaments. Biol Reprod 38:100–108
38. **Denkova R, Ivanov I, Dimitrova M** 1992 Microtubules and regulation of granulosa cell steroidogenesis by porcine granulosa cell conditioned medium. Endocr Regul 26:195–199
39. **Chen TT, Massey PJ, Caudle MR** 1994 The inhibitory action of taxol on granulosa cell steroidogenesis is reversible. Endocrinology 134:2178–2183
40. **Cameron MR, Caudle MR, Sullivan Jr WR, Peluso JJ, Wimalasena J** 1995 The steroidogenic and morphological effects of paclitaxel on cultured ovarian cancer cells. Oncol Res 7:145–156
41. **Wang TH, Popp DM, Wang HS, Saitoh M, Mural JG, Henley DC, Ichijo H, Wimalasena J** 1999 Microtubule dysfunction induced by paclitaxel initiates apoptosis through both c-Jun N-terminal kinase (JNK)-dependent and -independent pathways in ovarian cancer cells. J Biol Chem 274:8208–8216

42. **Dong C, Li Z, Alvarez R, Feng XH, Goldschmidt-Clemont PJ** 2000 Microtuble binding to smads may regulate TGFβ activity. Mol Cell 5:27–34
43. **Brodie A, Long B, Lu Q** 1998 Aromatase expression in the human breast. Breast Cancer Res Treat 49(Suppl 1):S85–S91, S109–S119
44. **Purohit A, Singh A, Ghilchik MW, Reed MJ** 1999 Inhibition of tumor necrosis factor α-stimulated aromatase activity by microtubule-stabilizing agents, paclitaxel and 2-methoxyestradiol. Biochem Biophys Res Commun 261:214–217
45. **Carter SD, Laskey JW** 1982 Effect of benomyl on reproduction in the male rat. Toxicol Lett 11:87–94
46. **Barnes TB, Verlangieri AJ, Wilson MC** 1983 Reproductive toxicity of methyl-1-(butylcarbamoyl)-2-benzimidazole carbamate (benomyl) in male Wistar rats. Toxicology 28:103–115
47. **Linder RE, Rehnberg GL, Strader LF, Diggs JP** 1988 Evaluation of reproductive parameters in adult male Wistar rats after subchronic exposure (gavage) to benomyl. J Toxicol Environ Health 25:285–298
48. **Spencer F, Chi L, Zhu MX** 1996 Effect of benomyl and carbendazim on steroid and molecular mechanisms in uterine decidual growth in rats. J Appl Toxicol 16:211–214
49. **Hess RA** 1998 Effects of environmental toxicants on the efferent ducts, epididymis and fertility. J Reprod Fertil 53(Suppl):247–259

***Endocrinology* is published monthly by The Endocrine Society (http://www.endo-society.org), the foremost professional society serving the endocrine community.**

0888-8809/04/$15.00/0
Printed in U.S.A.

Molecular Endocrinology 18(1):127–141

doi: 10.1210/me.2003-0110

Protein Kinase A Potentiates Adrenal 4 Binding Protein/Steroidogenic Factor 1 Transactivation by Reintegrating the Subcellular Dynamic Interactions of the Nuclear Receptor with Its Cofactors, General Control Nonderepressed-5/Transformation/ Transcription Domain-Associated Protein, and Suppressor, Dosage-Sensitive Sex Reversal-1: a Laser Confocal Imaging Study in Living KGN Cells

WUQIANG FAN, TOSHIHIKO YANASE, YIN WU, HISAYA KAWATE, MASAYUKI SAITOH, KOICHI OBA, MASATOSHI NOMURA, TAIJIRO OKABE, KIMINOBU GOTO, JUNN YANAGISAWA, SHIGEAKI KATO, RYOICHI TAKAYANAGI, AND HAJIME NAWATA

Department of Medicine and Bioregulatory Science (W.F., T.Y., M.S., K.O., M.N., T.O., K.G., H.N.) and Department of Geriatric Medicine (W.Y., H.K., R.T.), Graduate School of Medical Science, Kyushu University, Fukuoka 812-8582, Japan; Institute of Applied Biochemistry (J.Y.), University of Tsukuba, Ibaraki 305-8572, Japan; CREST (T.Y., Y.W., M.N., T.O., K.G., S.K., R.T., H.N.), Japan Science and Technology, Saitama 332-0012, Japan; and Institute of Molecular and Cellular Biosciences (S.K.), Graduate School of Agricultural and Life Sciences, University of Tokyo, Tokyo 113-0032, Japan

The mechanism through which protein kinase A (PKA) potentiates the transactivation ability of adrenal 4 binding protein/steroidogenic factor 1 (Ad4BP/SF-1) is currently unclear. In the present study, we investigated the mechanism by applying laser confocal microscopy and fluorescence recovery after photobleaching technique. In KGN cells, forskolin (a PKA stimulator) could reorganize wild-type Ad4BP/SF-1, but not mutant Ad4BP/SF-1 (G35E), from a diffuse distribution pattern to foci formation in the nucleus. The subcellular distributions of GCN5 (general control nonderepressed) and TRRAP (transformation/transcription domain-associated protein), both of which were recently proved to be working in the same complex as the third class of nuclear receptor coactivators, were unexpectedly diffuse inside and outside the nucleus, respectively, when they were separately transfected. However TRRAP was translocated into the nucleus in the presence of GCN5, and together with GCN5 colocalized with Ad4BP/SF-1 in the same foci when PKA was activated. A luciferase assay also indicated that these two cofactors enhanced Ad4BP/SF-1 transactivation.

Dosage-sensitive sex reversal (DAX-1) interacts with and thus inhibits Ad4BP/SF-1 transactivation. The coexistence of the two proteins dramatically altered their respective subnuclear distributions. They colocalized extensively, suggestive of binding, and Ad4BP/SF-1 was sharply immobilized when DAX-1 was coexpressed, whereas PKA could maintain mobility, as evidenced by Fluorescence Recovery After Photobleaching showing that Ad4BP/SF-1 mobility recovered after forskolin treatment.

Therefore, the PKA signal pathway may modify the interaction between Ad4BP/SF-1 and its activators and repressor (GCN5 and TRRAP are integrated, whereas DAX-1 is disassociated), and thus stimulate the Ad4BP/SF-1 transactivation. (*Molecular Endocrinology* 18: 127–141, 2004)

AD4BP, ALSO KNOWN as SF-1 and formally designated NR5A1 (nuclear receptor subfamily 5, group A, member 1) is a mammalian homolog of *Drosophila* fushi-tarazu factor 1 (1). Ad4BP/SF-1 was originally identified as a steroidogenic tissue-specific transcription factor (2) and belongs structurally to a member of the nuclear receptor superfamily that includes receptors for steroid, thyroid, and retinoid hormones. Ad4BP/SF-1 contains a characteristic zinc finger DNA-binding domain, an intervening hinge region, and a putative carboxyl-terminal ligand-binding domain. Ad4BP/SF-1 is designated as an orphan nuclear receptor because no definite ligand has been identified to date. Ad4BP/SF-1 is essential for the development of steroidogenic tissue (3–5) because disruption of mouse Ad4BP/SF-1 caused a lack

***Molecular Endocrinology* is published monthly by The Endocrine Society (http://www.endo-society.org), the foremost professional society serving the endocrine community.**

of adrenal and gonadal development, XY sex reversal, persistence of Müllerian structure in males, and abnormalities of the hypothalamus and pituitary gonadotropes (6, 7). In humans, there have been three patients reported thus far with Ad4BP/SF-1 mutations. The first Ad4BP/SF-1 mutation in humans was a heterozygous mutation (G35E) in a karyotypically male patient who showed complete XY sex reversal and primary adrenal failure (8).

Dosage-sensitive sex reversal (DAX-1) is an unusual orphan receptor with an expression profile that overlaps that of Ad4BP/SF-1, namely, in the hypothalamus-pituitary-adrenal and gonadal axis (9, 10). Naturally occurring loss-of-function mutations of the DAX-1 gene cause the human disorder adrenal hypoplasia congenital (AHC) and hypogonadotropic hypogonadism. DAX-1 is an inhibitor of steroidogenesis because it suppresses the transcriptional activation induced by Ad4BP/SF-1. One mechanism for suppression of the Ad4BP/SF-1 transactivation by DAX-1 is that DAX-1 can recruit the nuclear receptor corepressor N-CoR to Ad4BP/SF-1, and this corepressor recruitment capability was found to be markedly diminished in some of the naturally occurring DAX-1 mutations in patients with AHC and hypogonadotropic hypogonadism (11).

It is well known that activation of the cAMP-protein kinase A (PKA) signal pathway can strongly potentiate Ad4BP/SF-1 transactivation activity. Ad4BP/SF-1 binds as a monomer to its responsive element located in the promoter of steroidogenic genes. Ad4BP/SF-1 has been shown to be able to greatly increase both the basal and cAMP-dependent promoter activity of steroidogenic genes, including *CYP17*, *CYP11A*, and *CYP19* genes (12–14) and *inhibin-α* promoter (15). However, the mechanism by which cAMP augments Ad4BP/SF-1-dependent transactivation activity has not been well elucidated.

In the presence of ligand, steroid receptors have been thought to remain statically bound to regulatory sites in the target genes. In contrast, the vast majority of nuclear proteins, including steroid/nuclear receptors, are now believed to be highly dynamic with a wide range of mobility (16, 17). Recent intensive studies of glucocorticoid receptor (GR) (18–20) and estrogen receptor (ER) (21, 22) revealed that receptors undergo continuous exchange between chromatin regulatory elements and the nucleoplasm compartment when ligand is constantly available. The ligand-induced steroid receptor-coactivator complex, and even the individual components of those complexes, also undergo rapid exchange (18, 22). GR cycles continuously on and off the chromatin target as demonstrated as a hit and run model, in which GR first binds to chromatin after ligand activation, recruits a remodeling activity, facilitates transcription factor binding, and is simultaneously lost from the template (20). Rapid exchange of a nuclear receptor with regulatory sites may have important consequences, because the dynamic receptor would be continuously available for modification by some second pathway, such as multicellular signal pathways, which may quickly modulate nuclear receptor activity. Nuclear receptors such as retinoid acid receptor and thyroid hormone receptor (TR) have also been proven to be moving rapidly in the nucleus (23), hinting the dynamic exchange process might be a general feature of many nuclear receptors. Ligand-binding and protein-protein interaction seem to affect the intracellular mobility of some nuclear receptors and thereby may contribute to their biological activity (23). High mobility is thought to be critical for nuclear receptors to exert their effects on transcription (21).

By taking advantage of the technique of laser confocal microscopy and fluorescence recovery after photobleaching (FRAP) study, we found that, in living granulosa-like KGN cells, activation of the PKA signal pathway altered the Ad4BP/SF-1 subnuclear distribution pattern, leading to the formation of fluorescent foci. This process was accompanied by the recruitment of a newly identified third class of nuclear receptor coactivator complex, the GCN5/TRRAP complex, and also the disassembly of DAX-1, which interacted with Ad4BP/SF-1 and immobilized Ad4BP/SF-1. Our data thus suggest that the reintegration of the protein-protein interaction between Ad4BP/SF-1 and its coactivators or its repressor protein, DAX-1, might be a possible mechanism explaining how PKA potentiates Ad4BP/SF-1 transactivation.

RESULTS

Ad4BP/SF-1 Is Critical for the Augmentation of Aromatase Promoter II (ArPII) by PKA

The expression of the *human cytochrome P45019 aromatase* gene in the ovary is specifically driven by ArPII, a well known target promoter of Ad4BP/SF-1 (24). FSH, via membrane G protein, can stimulate aromatase expression in ovarian granulosa cells by increasing the intracellular cAMP level and thus activating the PKA signal pathway. Activation of the PKA pathway inside the cells can further increase the Ad4BP/SF-1-stimulated ArPII activity. As shown in Fig. 1, the steroidogenic human granulosa-like cell line KGN, which expresses aromatase, and the nonsteroidogenic NIH-3T3 fibroblast cell line were transfected with the human ArPII firefly luciferase reporter plasmid, pGL3-ArPII, together with the renilla luciferase plasmid phRL-CMV, which constitutively expresses the renilla luciferase to serve as an internal control. The expression vectors for wild-type or mutant

Abbreviations: Ad4BP/SF-1, Adrenal 4 binding protein/steroidogenic factor 1; AF-2 domain, activation function-2 domain; AHC, adrenal hypoplasia congenital, X-linked; AR, androgen receptor; ArPII, aromatase promoter II; CFP, cyan fluorescence protein; DAX-1, dosage-sensitive sex reversal; DMSO, dimethylsulfoxide; ER, estrogen receptor; FRAP, fluorescence recovery after photobleaching; GCN5, general control nonderepressed; GFP, green fluorescence protein; GR, glucocorticoid receptor; HI, heterogeneity index; PGC-1, peroxisome proliferators activated receptor-γ coactivator 1; PKA, protein kinase A; TRRAP, transformation/transcription domain-associated protein; YFP, yellow fluorescence protein.

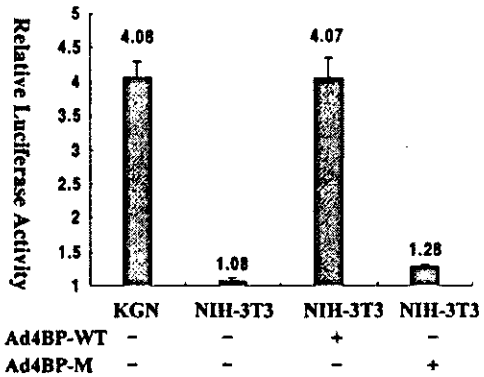

Fig. 1. CYP19 (Aromatase) Promoter II Activity in Response to Wild-Type or Mutant Ad4BP/SF-1 Stimulated by PKA

KGN cells and NIH-3T3 cells were transfected with the human ArPII firefly luciferase reporter plasmid, pGL3-ArPII, together with the renilla luciferase plasmid, phRL-CMV, as an internal control. pcDNA3.1-Ad4BP/SF-1-WT (wild type) or pcDNA3.1-Ad4BP/SF-1-M (mutant, G35E) was cotransfected into two groups of NIH-3T3 cells as indicated. All cells were treated overnight with either 10^{-6} mol/liter forskolin or the solvent DMSO. The multiple of relative luciferase activities induced by forskolin to that of control (induced by DMSO) are expressed as the mean ± SD.

(G35E) human Ad4BP/SF-1, or the control empty vector pcDNA3.1(+), were also cotransfected into NIH-3T3 cells. One night after the transfection, cells were treated overnight with 10^{-6} mol/liter forskolin (an adenyl cyclase stimulator that activates the PKA signal pathway by increasing cAMP) or the solvent dimethylsulfoxide (DMSO), and then a dual-luciferase assay was performed. In KGN cells, which endogenously express Ad4BP/SF-1, treatment with 10^{-6} mol/liter forskolin overnight increased the promoter activity 4-fold under the current experimental condition. On the other hand, in the nonsteroidogenic NIH-3T3 cells, which do not endogenously express Ad4BP/SF-1, the same treatment exhibited almost no effect on the ArPII activity. However, when wild-type Ad4BP/SF-1 was cotransfected into NIH-3T3 cells, overnight forskolin treatment elevated the ArPII activity 4-fold, as observed in KGN cells, whereas the transactivationally inactive mutant Ad4BP/SF-1 (G35E) could not convey the stimulatory effect of forskolin to ArPII (Fig. 1). Therefore, it is evident that Ad4BP/SF-1 is actually a requirement for the augmentation of ovarian ArPII activity induced by PKA. A similar effect of PKA on Ad4BP/SF-1-dependent transcription of the CYP 11A promoter was also observed in another pair of steroidogenic and nonsteroidogenic cells, Y1 and CV1 (data not shown).

Activation of PKA Altered the Subnuclear Distribution Pattern of Human Ad4BP/SF-1 from Homogeneity to Foci Formation

Research using nuclear receptors fused to green fluorescent protein (GFP), yellow fluorescent protein (YFP), or cyan fluorescent protein (CFP) under various stimuli in living cells has proved to be a powerful tool for deepening our understanding of the transcriptional activation of nuclear receptors (25). In this study, the intracellular distribution pattern of wild-type, or mutant Ad4BP/SF-1 containing G35E, in response to PKA, was examined dynamically by observing the fusion proteins GFP-Ad4BP/SF-1 and YFP-Ad4BP/SF-1 under a confocal laser microscope. The functional validity of these chimeric proteins was tested by a dual luciferase assay using the pGL3-ArPII reporter described above in KGN cells. As shown in Fig. 2, the transactivation activity of GFP-Ad4BP/SF-1-WT (wild type) was up to 87% conserved compared with pcDNA3.1-SF1-WT, and the responsiveness of GFP-SF1-WT to PKA was almost completely conserved. Both GFP-Ad4BP/SF-1-M (mutant) and pcDNA3.1-Ad4BP/SF-1-M were transactivationally inactive compared with Ad4BP/SF-1-WT.

After transient transfection, and treatment with or without 10^{-6} mol/liter forskolin, the intracellular distribution of each variant of Ad4BP/SF-1 fused to GFP was visualized in both steroidogenic KGN cells and nonsteroidogenic monkey kidney CV1 cells using a LSM-510-META laser confocal scanning microscope (Carl Zeiss, Oberkochen, Germany). GFP-Ad4BP/SF-1-WT (Fig. 3A) was predominantly located inside the nuclei, as previously reported in Y1 cells (26). The nucleoli demonstrated almost no fluorescence, suggesting that nucleoli are almost devoid of Ad4BP/SF-1. The cytoplasm was also devoid of fluorescence. In the absence of forskolin, the GFP-Ad4BP/SF-1-WT

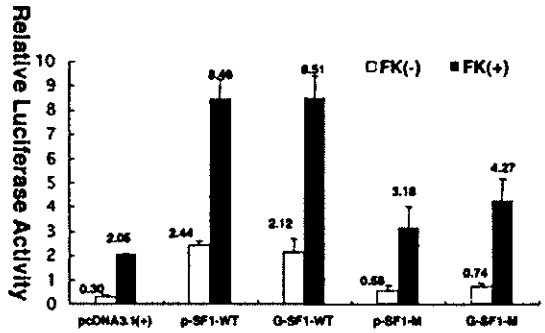

Fig. 2. Transactivation Activity of Wild-Type or Mutant Ad4BP/SF-1 Fused to GFP and Their Responsiveness to PKA

KGN cells were transfected with pcDNA3.1-Ad4BP/SF-1-WT or pcDNA3.1-Ad4BP/SF-1-M (G35E) or their respective GFP-fusion plasmids together with pGL3-ArPII + phRL-CMV. The cells were then treated overnight with 10^{-6} mol/liter forskolin or the solvent DMSO. *Solid and hollow bars* represent the luciferase activities with treatment of forskolin or DMSO, respectively. The transactivation activity of GFP-Ad4BP/SF-1-WT was preserved up to 87% compared with pcDNA3.1-Ad4BP/SF-1-WT, and its responsiveness to forskolin was almost completely conserved. Both pcDNA3.1-Ad4BP/SF-1-M and GFP-Ad4BP/SF-1-M were transactivationally inactive.

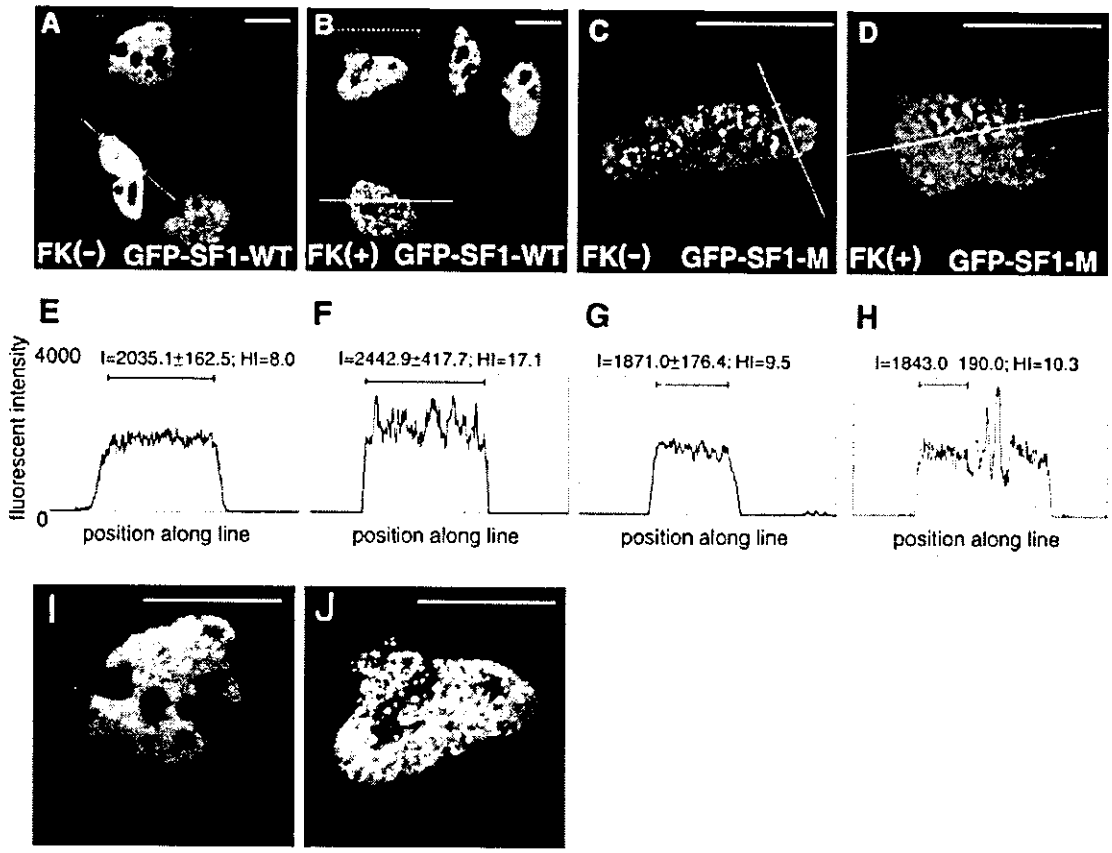

Fig. 3. Subnuclear Localization of GFP-Ad4BP/SF-1-WT and GFP-Ad4BP/SF-1-M in the Presence or Absence of 10^{-6} mol/liter Forskolin

KGN cells were transfected with 0.5μg/dish of GFP-Ad4BP/SF-1-WT (A and B) or GFP-Ad4BP/SF-1-M (C and D). The chimeric fluorescent proteins expressed were observed in living cells using a Zeiss LSM 510 META laser confocal microscope as described in *Materials and Methods*. Wild-type Ad4BP/SF-1 is diffuse in the nucleus (A and I) and is assembled into foci on a diffuse fluorescence background when PKA is activated (B and J). Mutant Ad4BP/SF-1 is diffuse in the nucleus whereas dots are manifested in the nucleoli (C), and forskolin has no effect on its distribution pattern (D). The lines for line scan analysis were shown on each representative cell, with the segment for HI (heterogeneity index) analysis also indicated. The fluorescent intensity fluctuation graph of each representative cell is shown as panels E–H, in relation to panels A–D, respectively. X axis is the position along lines and Y axis is fluorescent intensity. A *bar within each graph* marks the segment of the line for which the HI analysis is performed; the corresponding I (intensity) and HI values are indicated on the *top* of each *graph*. Panels I and J are magnified views of the cells outlined by the *hatched line* in panel A and B, respectively. *Magnification scale bar*, 10 μm.

fluorescence signal was quite diffuse in the nuclei of most cells (Fig. 3, A and I).

The treatment of 10^{-6} mol/liter forskolin overnight caused more than 60% of studied cells to manifest clear foci formation, which happened inside the nucleoplasm but not the nucleoli (Fig. 3, B and J), suggesting an intranuclear rearrangement of the Ad4BP/SF-1 distribution pattern induced by PKA. The intranuclear distribution pattern of GFP-Ad4BP/SF-1-WT was further quantitatively analyzed. Digital figures obtained by a LSM-510-META microscope were subjected for Linescan analysis by the LSM software (version 3.0). A straight line was made through a target cell, and the fluorescent intensity along the line was recorded by the software. The mean and SD values of the fluorescent intensity signals for the segment of interest (nucleus, avoid nucleoli) were calculated. The heterogeneity of fluorescent intensity along the segment of interest was evaluated by the parameter of HI (heterogeneity index), which was calculated by the formula of HI = 100 × SD/mean. A fluorescent intensity fluctuation graph, which apparently demonstrates the heterogeneity, was made by plotting intensity against distance of the line. Panels E–H of Fig. 3 represent the Linescan of panels A–D, respectively. As shown in Fig. 3E, the fluorescent intensity of the representative cell from forskolin(−) group remains quite constant (HI = 8.0), whereas forskolin treatment (Fig. 3F) causes a 2-fold fluorescent intensity increase (HI = 17.1), indicating the reorganization of GFP-Ad4BP/SF-1-WT in the nuclear. Fifty cells with proper expression of GFP-Ad4BP/SF-1-WT from each group were analyzed by

Linescan, and the HI value of the forskolin (+) group is more than two times higher than that of the forskolin (−) group (17.9 ± 3.07 *vs.* 7.9 ± 1.7, $P < 0.01$).

However, on transfection with GFP-Ad4BP/SF-1-M (mutant), the fluorescence signal was still found to localize inside the nucleus in the absence of forskolin (Fig. 3C), but it was also diffusely distributed even in the presence of 10^{-6} mol/liter forskolin (Fig. 3D). Linescan shows that the intranuclear distribution pattern is almost not altered by forskolin (Fig. 3, G and H). Interestingly, clear fluorescent dots were observed inside the nucleoli in the case of the mutant, and the pattern was unchanged in the presence or absence of forskolin.

The similar phenomenon could be observed in CV1 cells (data not shown). Precisely, a time course study found that, in KGN cells, wild-type Ad4BP/SF-1 made foci within 3 h after addition of forskolin, while in CV1 cells, only a small amount of cells began manifesting foci 5–6 h after forskolin treatment, indicating a delayed reaction of Ad4BP/SF-1 to PKA signal pathway in this cell line as compared with the KGN cell line.

Coactivators GCN5 and TRRAP Are Recruited to Ad4BP/SF-1 Foci When the PKA Signal Pathway Is Activated

Foci formation in the nuclear localization of nuclear receptors usually correlated with a functionally active state of the nuclear receptors as a result of a compartmental shift upon activation of the nuclear receptors (25). Activation of PKA seems to provoke the assembly of wild-type Ad4BP/SF-1 protein into this active foci state but had no effect on the mutant Ad4BP/SF-1, which could not respond transactivationally to PKA (Fig. 1). The question to be addressed next is the nature of this foci formation of Ad4BP/SF-1 induced by PKA. Coactivators such as p300/CBP (CREB-binding protein), SRC-1 (steroid receptor coactivator-1), and GCN5 exhibit HAT (histone acetyltransferase) activity. These HAT proteins acetylate nucleosomal histone, which further increases the accessibility of transcription factors to their DNA targets. Recently, it has been pointed out that not only histone, but also several transcription factors such as p53, E2F transcription factor 1, and AR *etc.*, can also be acetylated by the HAT coactivators. GCN5 was found to be able to acetylate Ad4BP/SF-1 *in vitro* and thus stimulate the transactivation of Ad4BP/SF-1 (27). GCN5 can be recruited to Ad4BP/SF-1 as a newly identified Ad4BP/SF-1 coactivator. The c-Myc-interacting protein TRRAP (28) was recently proved to be working together with the coactivator GCN5 and other partners such as TAFII30 (29) as the third class of coactivator complex for nuclear receptors in addition to the first class of the p160/CBP-HAT coactivator complex and the second vitamin D receptor interacting protein/thyroid hormone receptor-associated protein non-HAT coactivator complex (30). The three LXXLL motifs of TRRAP serve as a direct and ligand-dependent interaction surface for nuclear receptors, *e.g.* ERα (30). As shown in Fig. 4, both GCN5 and TRRAP were found to further potentiate the Ad4BP/SF-1-stimulated ArPII activity with a more powerful effect seen in the case of TRRAP. Both of these factors may work as coactivators for Ad4BP/SF-1 and enhance the transactivation ability of Ad4BP/SF-1.

We next studied the intracellular distribution dynamics of both GCN5 and TRRAP in living KGN cells and their relationship with Ad4BP/SF-1 in the presence or absence of activation of the PKA signal pathway. The transcriptional coactivation ability of these fusion proteins measured by the dual-luciferase reporter assay was similar to that observed in Fig. 2 (data not shown). Considering that the PKA pathway is a critical signal pathway for cells, autonomous activation of this pathway might interfere with the results and thus possibly make the difference less obvious. Therefore, for the control groups of cells, we blocked the PKA pathway with 10^{-6} mol/liter H89, seeking a clearer difference between the control and forskolin groups. When GFP-GCN5 was transfected into KGN cells, fluorescence was mainly located inside the nucleus in a uniform pattern with the nucleoli being devoid of fluorescence. This distribution pattern was not altered even after PKA was stimulated by 10^{-6} mol/liter forskolin (Fig. 5, A and B). When TRRAP-GFP was transfected into KGN cells, TRRAP-GFP predominantly resided in the cytosol in a diffuse manner, and again 10^{-6} mol/liter forskolin had no effect on this distribution manner (Fig. 5, C and D). To verify this result, TRRAP-GFP was also transfected into the nonsteroidogenic NIH-3T3 cells, and the same result was observed (Fig. 5, E and F). This observation of dissociated localization between GCN-5 and TRRAP in the basal state was unexpected because TRRAP/GCN5 has been shown to work as cofactor in the same complex. When we next cotransfected both GFP-GCN5 and TRRAP-YFP into KGN cells, the distribution pattern of GCN5 was almost identical to the one observed when GFP-GCN5 was

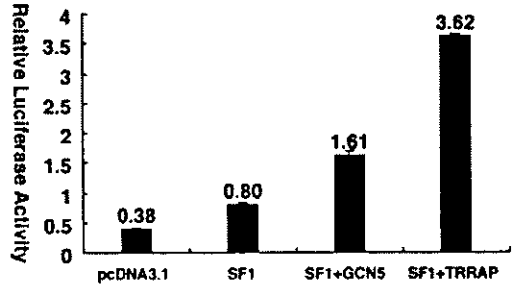

Fig. 4. Coactivators GCN5 and TRRAP Potentiate the Transactivation Activity of Ad4BP/SF-1 on the CYP19 Promoter

NIH-3T3 cells were transfected with pGL3-ArPII + phRL-CMV. pcDNA3.1-Ad4BP/SF-1-WT, or in combination with the same amount on a molar basis of either pcDNA3-GCN5 or pcDNA3-TRRAP were also cotransfected. Both cofactors could potentiate Ad4BP/SF-1-mediated transcription.

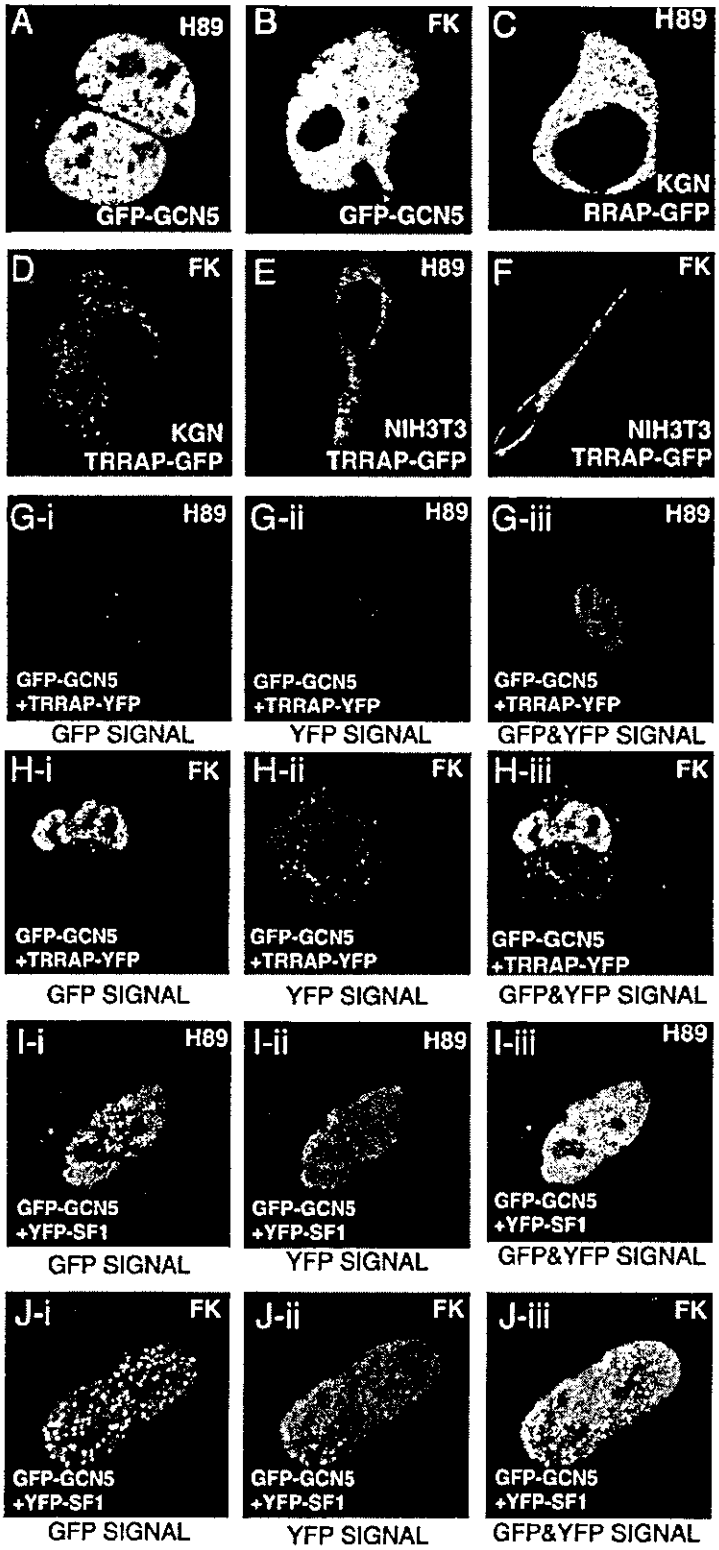

Fig. 5. Subcellular Localization of Fluorescent Protein-Fused GCN5 or Fluorescent Protein-Fused TRRAP, and Their Interrelationship with Fluorescent Ad4BP/SF-1, with the PKA Signal Pathway Either Blocked by H89 or Activated by Forskolin

KGN cells or NIH-3T3 cells (panels E and F) were transfected with the expression plasmids indicated in each panel. The

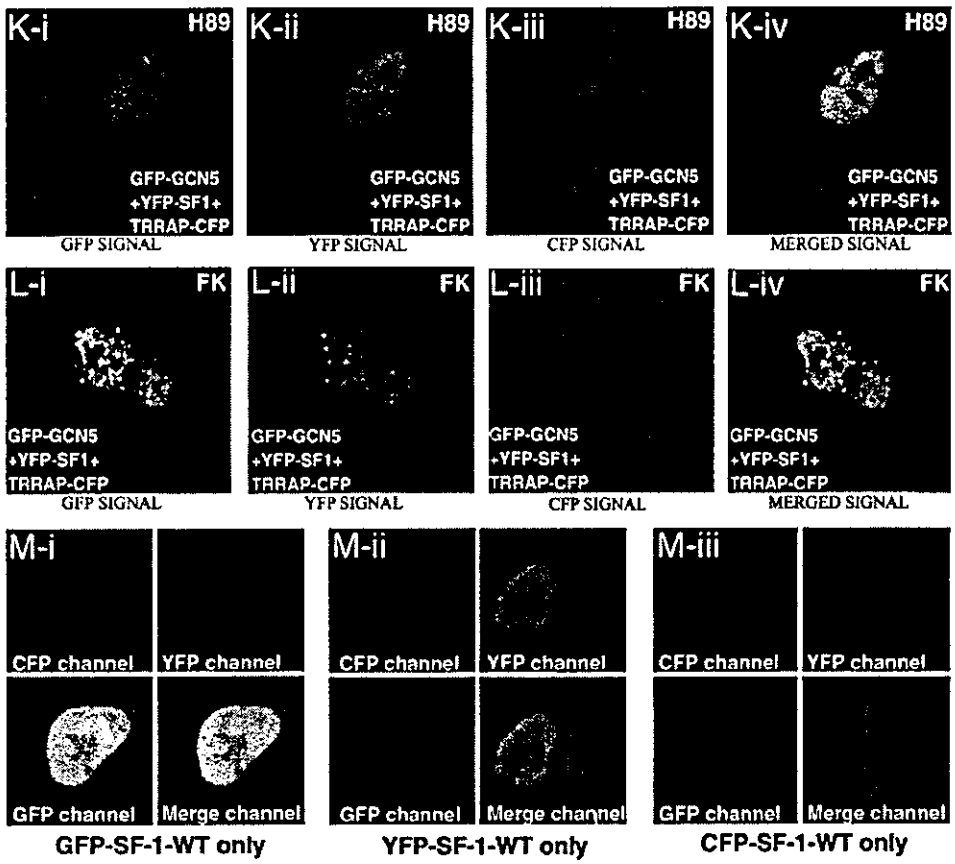

Fig. 5 Continued.

solely transfected. However, in contrast to the restricted localization of TRRAP in the cytosol when TRRAP-GFP was solely transfected, TRRAP-YFP with the coexistence of GFP-GCN5 resided homogenously both inside and outside the nucleus, with a little more intensity inside the nucleus (Fig. 5G). This pan-cellular distribution of TRRAP with the coexistence of GCN5 was unchanged by 10^{-6} mol/liter forskolin treatment (Fig. 5H). TRRAP may originate as a cytoplasmic protein, but GCN5 might be able to bind TRRAP and drag it into the nucleus, and then both work together as coactivators in the same complex.

The intracellular distribution relationships between GCN5, TRRAP, and Ad4BP/SF-1 in the presence and absence of PKA activation were subsequently studied. When GFP-GCN5 and YFP-Ad4BP/SF-1 were cotransfected into KGN cells, both fluorescence signals were predominantly located in the nucleus in a uniform pattern (Fig. 5I). Forskolin (10^{-6} mol/liter) changed YFP-Ad4BP/SF-1 to a speckled distribution pattern with the formation of foci. Furthermore, GFP-GCN5 was also induced to make foci by forskolin treatment and precisely colocalized with YFP-Ad4BP/SF-1 in the same fluorescent foci (Fig. 5J). When GFP-GCN5, YFP-Ad4BP/SF-1, and TRRAP-CFP were cotransfected together in the presence of a PKA blocker, H89, both GFP-GCN5 and YFP-Ad4BP/SF-1 showed a diffuse distribution pattern in the nucleus while TRRAP-

amounts of each plasmid transfected in each panel were equivalent on a molar basis. Treatment with forskolin (FK) or H89 is indicated *in or just below each panel*. In the cases of multifluorescent protein chimeras cotransfection, each fluorescent signal and the merged signals are also indicated. GCN5 is diffuse in the nucleus (A and B) of KGN cells, whereas TRRAP is predominantly located in the cytoplasm in both KGN cells (C and D) and NIH-3T3 cells (E and F). TRRAP is dragged into the nucleus when GCN5 is also present (G and H). Forskolin has no effect on their distribution pattern. When cotransfected with Ad4BP/SF-1, GCN5 (I and J) and GCN5 and TRRAP together (K and L) were recruited to Ad4BP/SF-1 foci when Ad4BP/SF-1 was activated by forskolin. M-i, M-ii, and M-iii are controls demonstrating the unmixing algorithms reliability of simultaneous imaging of GFP, YFP, and CFP. Cells containing only GFP are clearly visible in only the GFP channel with no bleed through in the YFP and CFP channels (M-i). Similarly, cells containing only YFP (M-ii) or CFP (M-iii) are only visible in the YFP or CFP channel, with no bleed through in the other two channels.

CFP was diffusely distributed in a pan-cellular manner (Fig. 5K). However, foci formation took place inside the nucleus when forskolin was added. In this case, not only GCN5 and Ad4BP/SF-1 were colocalized in fluorescent dots, but TRRAP also made foci and finely colocalized with GCN5 and Ad4BP/SF-1 (Fig. 5L). These data suggest that PKA activation assembles Ad4BP/SF-1 into foci with an accompanying recruitment of coactivators like the GCN5/TRRAP complex.

DAX-1 Immobilized Ad4BP/SF-1 in the Nucleus, and this Process Was Rescued by PKA

DAX-1 is a suppressive protein for the transcriptional activation induced by Ad4BP/SF-1 and is thus considered to be an inhibitor of steroidogenesis. It has been proved that DAX-1 can bind directly to Ad4BP/SF-1 and antagonize the transcriptional activity of Ad4BP/SF-1, either via its silencing C-terminal domain (31) or by recruiting the corepressors N-CoR (11) or Alien (32) to Ad4BP/SF-1. We investigated the relationship between DAX-1 and Ad4BP/SF-1 during the process of activation of Ad4BP/SF-1 induced by PKA. The dual-luciferase assay revealed that the inhibition of the transcriptional activity of Ad4BP/SF-1 induced by DAX-1 could be recovered by PKA stimulation (Fig. 6). Next, the subcellular distributions of GFP-DAX-1 alone, and combined with YFP-Ad4BP/SF-1, were studied in living KGN cells the PKA signal pathway of which was either blocked or activated. When the cells were transfected by GFP-DAX-1 alone, the fluorescence signal was predominantly located in the nucleus in a homogenous manner, while a relatively weak diffuse fluorescence was observed in the cytosol (Fig. 7A). Forskolin (10^{-6} mol/liter) treatment caused no effect on this distribution pattern of DAX-1 (Fig. 7B). The same distribution pattern of endogenous DAX-1 in KGN cells was observed by immunostaining (data not shown). However, cotransfection of GFP-DAX-1 and YFP-Ad4BP/SF-1 caused a dramatic change in the subcellular distribution patterns. Namely, both proteins assembled to form clear dots with no visible diffuse fluorescent background, and the GFP-DAX-1 and YFP-Ad4BP/SF-1 fluorescent dots completely overlapped (Fig. 7C, i, ii, and iii). This was further supported by the LSM semiquantitative colocalization analysis (Fig. 7C, iv). The weak GFP signal observed in the cytosol when GFP-DAX-1 was solely transfected also completely disappeared (Fig. 7C). More importantly, the completely overlapping GFP-DAX-1 and YFP-Ad4BP/SF-1 fluorescence signals were partially separated when the cells were stimulated by 10^{-6} mol/liter forskolin (Fig. 7D). The LSM colocalization analysis showed that the incomplete colocalization resulted from partial GFP-DAX-1 signal being disassociated from the overlapping dots (Fig. 7D, iv). This phenomenon was observed in most cells with proper expression of both GFP-DAX-1 and YFP-Ad4BP/SF-1, although it has been observed that different individual cells respond to forskolin stimulation to a variable extent (data not shown). Thus interaction between DAX-1 and Ad4BP/SF-1 might be interfered with or weakened by activation of PKA, and DAX-1 might be stripped from binding with Ad4BP/SF-1 when PKA is activated.

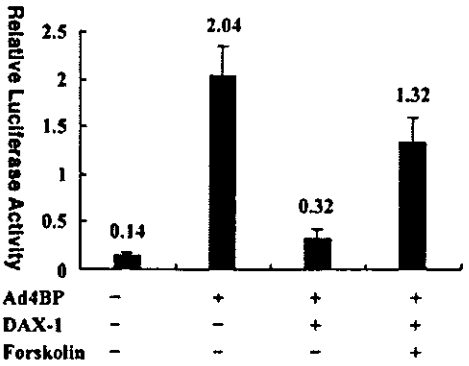

Fig. 6. Effect of Forskolin on DAX-1-Mediated Inhibition of Ad4BP/SF-1 Transactivation

KGN cells were cotransfected with pGL3-ArPII and phRL-CMV. The strategy for cotransfection of Ad4BP/SF-1, DAX-1, or both, and the treatment with forskolin are indicated. DAX-1 could repress Ad4BP/SF-1-mediated transcription, whereas the DAX-1-inhibited Ad4BP/SF-1 transactivation could be rescued by forskolin.

To further investigate this hypothesis, we applied the FRAP technique to examine the intranuclear dynamics of fluorescent Ad4BP/SF-1 and DAX-1 in living KGN cells. Proper mobility has recently been shown to be important for nuclear receptors to be transactivationally functional (21). As shown in Fig. 8, coexpression of pRc/RSV-DAX-1 not only changed the subnuclear distribution pattern of YFP-Ad4BP/SF-1, but also clearly immobilized YFP-Ad4BP/SF-1. When PKA was blocked, the half-maximal recovery time ($t_{1/2}$) of YFP-Ad4BP/SF-1 with no cotransfection of DAX-1 was 0.84 ± 0.16 sec (mean ± SD, n =20, Fig. 8A), whereas the recovery $t_{1/2}$ of YFP-Ad4BP/SF-1 with cotransfection of DAX-1 was prolonged to 9.21 ± 2.36 sec (mean ± SD, n =20, Fig. 8B). These data strongly suggest that Ad4BP/SF-1 is quite mobile in the nucleus, and interaction of the receptor with DAX-1 may interfere with its mobility. Immobilization of Ad4BP/SF-1 might also be a mechanism through which DAX-1 exerts its inhibitory effect on Ad4BP/SF-1, in addition to the mechanism of direct interaction and recruitment of corepressors. We further studied the mobility of YFP-Ad4BP/SF-1 with the coexpression of DAX-1 with forskolin to activate the intracellular PKA pathway. Interestingly, the sharply reduced mobility of YFP-Ad4BP/SF-1 induced by DAX-1 partially recovered in the presence of forskolin (recovery $t_{1/2}$: 1.78 ± 0.34 sec, mean ± SD, n =20, Fig. 8C). From these data, activation of PKA might be able to disrupt or weaken the direct interaction of the inhibitory DAX-1 with Ad4BP/SF-1 and thus potentiate the transactivation

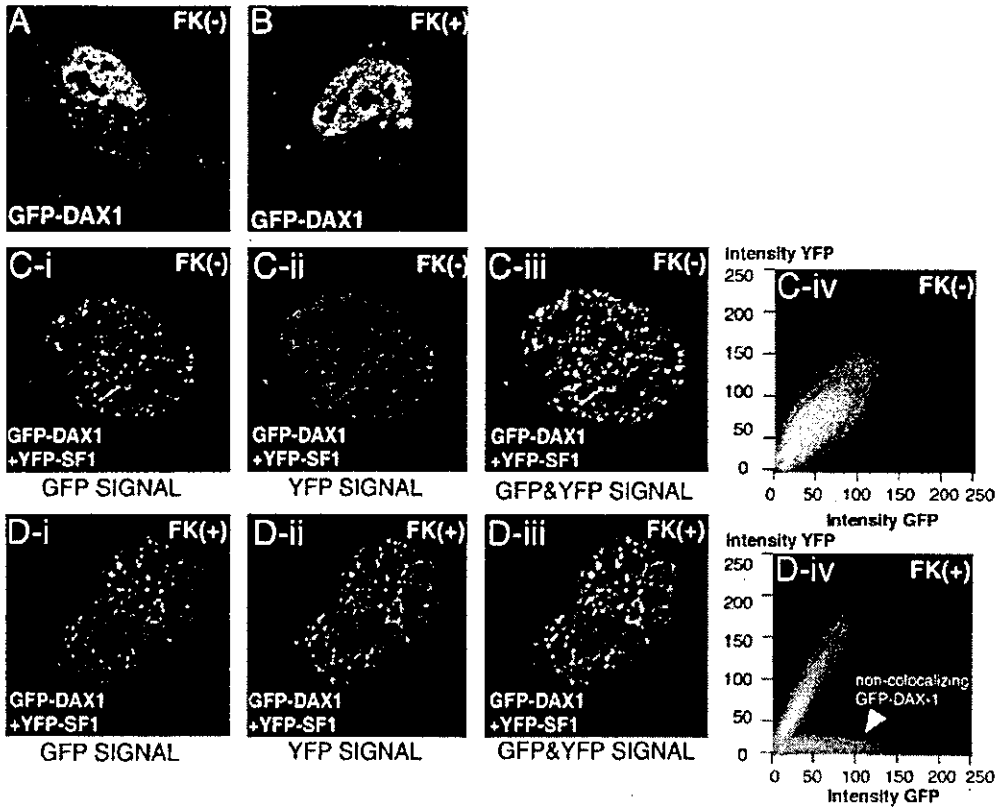

Fig. 7. Subcellular Distribution Interaction between GFP-DAX-1 and YFP-Ad4BP/SF-1

KGN cells were transfected with GFP-DAX-1 or GFP-DAX-1 + YFP-Ad4BP/SF-1 as indicated in each panel. A and B, DAX-1 is mainly diffuse in the nucleus with a weak signal detected in the cytoplasm, and this distribution is not altered by forskolin. C, Coexistence of GFP-DAX-1 and YFP-Ad4BP/SF-1 leads to the formation of clear dots with both fluorescent signals overlapping each other. The LSM colocalization analysis (C-iv) shows that GFP-DAX-1 and YFP-Ad4BP/SF-1 signals are colocalizing almost completely. No diffuse intranuclear fluorescence background or weak cytosol fluorescence was detected. D, Forskolin partially separated the two completely overlapping fluorescent signals The colocalization analysis (D-iv) shows that a fraction of GFP-DAX-1 signal is not colocalizing with YFP-Ad4BP/SF-1, suggesting that the interaction between Ad4BP/SF-1 and DAX-1 is weakened, and partial DAX-1 is disassociated from the Ad4BP/SF-1-DAX-1 binding complex.

of Ad4BP/SF-1, as shown by the luciferase reporter assay in Fig. 6.

DISCUSSION

Various lipophilic ligands have been found to interact with ligand-binding domains, induce allosteric changes, and thus convert nuclear receptors into an active conformation that can actively regulate transcription. However, Ad4BP/SF-1 is an orphan nuclear receptor and has no known ligand. Cross-talk with the main intracellular signal transduction pathways and protein-protein interactions seem to play definitive roles in the transcriptional regulation by nuclear receptors, especially those orphan nuclear receptors like Ad4BP/SF-1.

It is well known that the transactivational activity of Ad4BP/SF-1 can be further activated by the cAMP-PKA signal pathway. In this study, this phenomenon was also observed in a well known Ad4BP/SF-1 target gene's promoter, *human CYP19* ArPII, in KGN cells. The precise mechanism by which cAMP potentiates Ad4BP/SF-1-dependent transactivation was investigated using this model. One hypothesis is that PKA may directly or indirectly activate Ad4BP/SF-1 transcriptional activity by phosphorylation of Ad4BP/SF-1 because Ad4BP/SF-1 has been demonstrated to be phosphorylated *in vitro* by the PKA or MAPK pathway (33, 34). However, mutations of the predicted potential phosphorylation sites for the PKA (Ser 430) and MAPK (Ser 203) pathways did not affect the ability of PKA to stimulate Ad4BP/SF-1-dependent transactivational activity (26). In fact, it was shown to be difficult to prove that elevated cAMP could stimulate the phosphorylation of Ad4BP/SF-1 *in vivo* (35). In this regard, the opposite theory has recently been proposed that during the process of PKA-mediated Ad4BP/SF-1

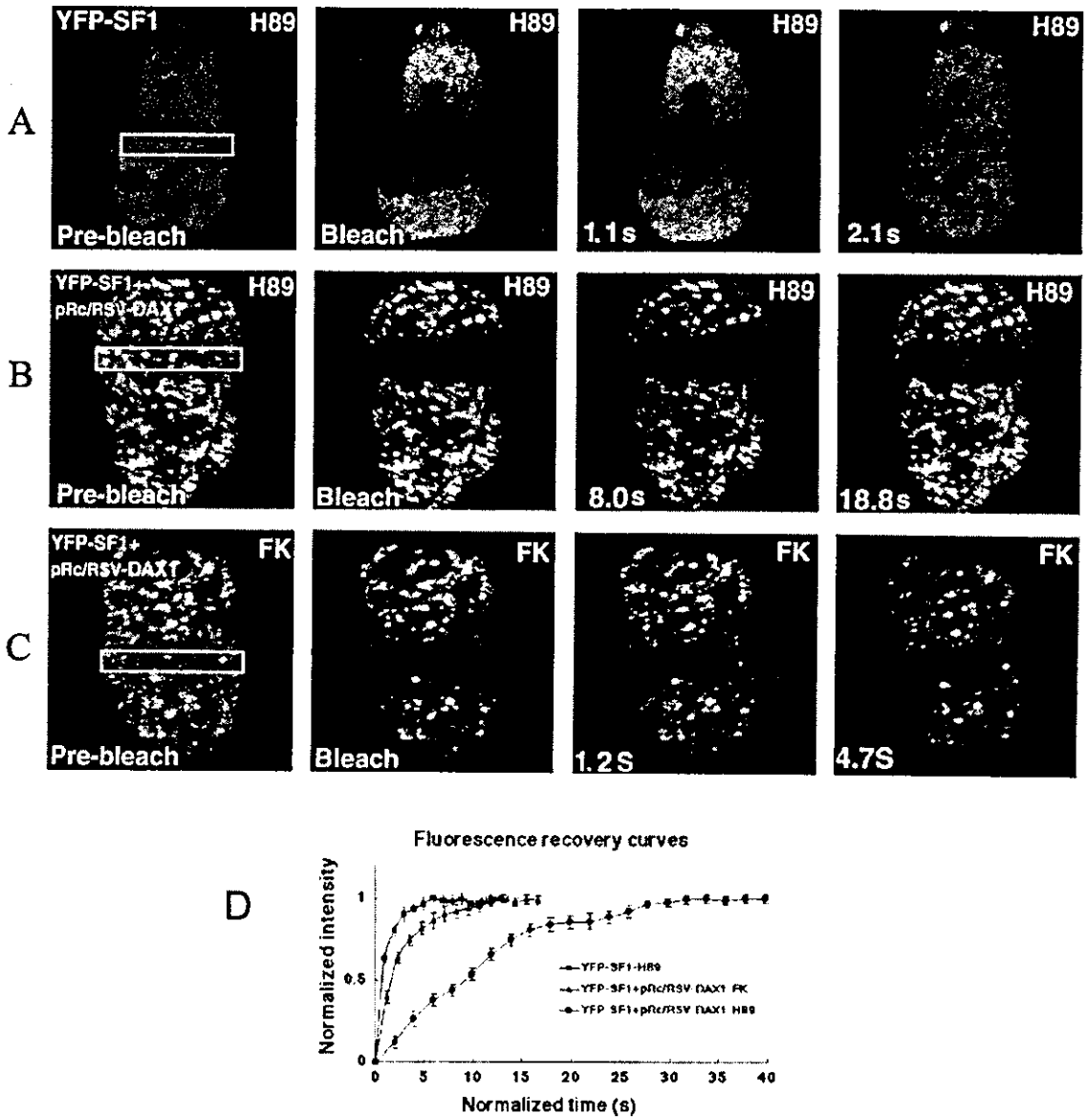

Fig. 8. FRAP Analysis of YFP-Ad4BP/SF-1 Cotransfected with pRc/RSV-DAX-1 after Forskolin or H89 Treatment

KGN cells were transfected with YFP-Ad4BP/SF-1 or YFP-Ad4BP/SF-1 + pRc/RSV-DAX-1, and treated with 10^{-6} mol/liter H89 or 10^{-6} mol/liter forskolin as indicated. Images show a single Z section and were obtained before and after bleaching at the time points indicated in each panel. The region of interest (ROI) of photobleaching is also indicated. A, When YFP-Ad4BP/SF-1 was solely transfected and cells were treated with H89, YFP-Ad4BP/SF-1 demonstrates a high intranuclear mobility. A definite bleach zone is detected after photobleaching. The total nuclear fluorescence reaches equilibrium within 1 sec. B, Cotransfection of pRc/RSV-DAX-1 and treatment with H89 prolonged the fluorescence recovery half-time to 9 sec, indicating that Ad4BP/SF-1 mobility is reduced. C, The prolonged fluorescence recovery time is rescued by forskolin. Ad4BP/SF-1 regains its mobility in the presence of forskolin, suggesting that PKA weakens the Ad4BP/SF-1-DAX-1 interaction. D, The recovery curves of the three groups of cells. The normalized intensity at each time point was averaged and plotted to the normalized time points. The $t_{1/2}$ value can be readily observed from the graph as the time at which the normalized intensity reaches 0.5 arbitrary units.

transactivation, phosphatase activity, but not kinase activity, may be critical (36). Another possible mechanism suggested was that PKA may increase the Ad4BP/SF-1 protein level by stabilizing it (26), but there is also conflicting evidence that the mRNA or protein level of Ad4BP/SF-1 remains constant after elevation or decrease of the cAMP level (37, 38). Peroxisome proliferators activated receptor-γ coactivator 1 (PGC-1) is an unique coactivator that can be transcriptionally increased by cAMP-PKA signaling (39).

The possibility that PKA may augment Ad4BP/SF-1 transactivation by means of increasing the PGC-1 level, if PGC-1 could serve as a coactivator for Ad4BP/SF-1, seems to be unlikely because forced expression of PGC-1 could not further enhance Ad4BP/SF-1-mediated ArPII activity in either KGN or NIH-3T3 cells (data not shown).

Ligand-induced subnuclear compartmentalization (foci formation) is a common phenomenon of nonorphan nuclear receptors and usually is considered to be related to the transactivationally active form of receptors. Ligand-induced transactivationally active GR (40), vitamin D receptor (41), estrogen receptor (ER) (42), mineralocorticoid receptor (43), and androgen receptor (AR) (44) have been found to be distributed in the nuclei that produce the GFP fluorescent foci. Intranuclear fluorescent foci formation depends closely on whether the receptor is transcriptionally active or inactive. Transcriptionally active AR treated with dihydrotestosterone produced 250–400 foci in the boundary region between euchromatin and heterochromatin (44). Although AR bound to antiandrogens like hydroxyflutamide also translocated to the nucleus, they spread homogeneously throughout the nucleus without producing any fluorescent foci (44). In addition, when ARs make foci, as induced by dihydrotestosterone, coactivators like SRC-1, TIF2, and CBP were found to be accumulated in identical locations, and CBP was found to be one of the factors essential for AR foci formation (25). It is thus speculated that transcriptionally activated nuclear receptors are transferred to common nuclear compartments (foci) in the nuclear matrix and form a complex with coactivators, and that this process is essential for full transactivation. However, it is unlikely that foci compartments directly represent the active transcription sites, because they were found usually not to overlap with activated RNA polymerase II or nascent mRNA. But currently, liganded GR has been observed to dynamically aggregate to an artificial promoter (a MMTV array that has been integrated to chromosome), where the biding sites are amplified many times (18, 19). Another corroborative study reported a strong correlation between aryl hydrocarbon receptor foci and the active transcription sites (45). Recent studies generally suggest that foci compartments of nuclear receptors may represent the sites for storage and/or assembly of activated nuclear receptor, and nuclear receptors can be dynamically recruited from foci compartments into the active transcription sites. It should be noted that foci are also possibly related to protein degradation compartment (46), because cognate ligand also induce proteolysis, a process that is tightly coupled with the ligand-induced activation and compartmentalization of nuclear receptors, and is believed to be a mechanism to precisely regulate the activity of liganded nuclear receptors.

In parallel with the elevated transactivation ability, GFP-Ad4BP/SF-1 underwent a compartmental shift and manifested foci formation in the nucleus when the PKA signal pathway was activated. This phenomenon was observed only with wild-type Ad4BP/SF-1, and not in the functionally inactive mutant Ad4BP/SF-1 (G35E). The PKA-inducible foci formation appears to be a characteristic of functionally stimulated Ad4BP/SF-1 because it is consistent with the PKA-stimulated transactivation of Ad4BP/SF-1, suggesting that Ad4BP/SF-1 is assembled to a transactivationally active subnuclear compartment. In addition, in the process of PKA-triggered foci formation, recruitment of coactivators such as GCN5 and TRRAP also takes place. It should be noted that this PKA-induced foci formation occurs on a diffuse fluorescence signal background, suggesting that not all Ad4BP/SF-1 proteins, but rather a fraction of them, are assembled to the foci, and that the Ad4BP/SF-1 in the nuclear pool may be undergoing rapid exchange.

The GCN5/TRRAP complex is a newly identified third class of nuclear receptor coactivator complex, in addition to the previously described P160/CBP HAT complex and vitamin D receptor-interacting protein/thyroid hormone receptor-associated protein non-HAT complex. GCN5 contains HAT activity whereas the three LXXLL motifs of TRRAP are responsible for interaction with nuclear receptors, according to the reported case of ERα, in a ligand-dependent manner (30). Based on our data, TRRAP is a surprisingly dominant cytoplasmic protein but seems to be dragged into the nucleus by its partner, GCN5. Both of these proteins can be recruited to Ad4BP/SF-1 when the receptor is stimulated by PKA, suggesting that this nuclear receptor coactivator complex is involved in the Ad4BP/SF-1 activation process. Therefore, activation of the PKA signal pathway is able to alter the subnuclear distribution pattern of Ad4BP/SF-1 and assemble this orphan nuclear receptor to a functionally active state, with recruitment of coactivators. Forskolin, a stimulator of adenyl cyclase, could induce Ad4BP/SF-1 to make foci, a phenomenon mimicking the role of cognate ligands to their respective nuclear receptors, raising a new concept that foci formation can also be a result of the activation of an intracellular signal pathway like PKA, which secondarily activates the nuclear receptors themselves. This result sheds new light on our understanding of the nature of foci, which has not yet been well defined.

The mutant Ad4BP/SF-1 (G35E) could not be transactivationally enhanced by PKA and could not make foci in the presence of forskolin. Surprisingly, however, mutant Ad4BP/SF-1 fluorescence aggregated in dots in the nucleoli. Although no significant nucleolar fluorescence was detectable in the case of the wild type, we cannot exclude the presence of a small fraction of Ad4BP/SF-1 molecules localizing to the nucleolus. The p-box of Ad4BP/SF-1, where the G35E mutation is located, or the region nearby, might be an important domain required for nuclear matrix binding of Ad4BP/SF-1 and thus prevent Ad4BP/SF-1 from entering the nucleoli, or this domain might be a nucleolus export

signal for the small fraction of Ad4BP/SF-1 that has entered the nucleolus to get out.

DAX-1 is able to interact directly with Ad4BP/SF-1 (31). The amino-terminal region of DAX-1 contains an interaction domain for Ad4BP/SF-1, and the C terminus of DAX-1 is itself transcriptionally silencing. In addition to the recruitment of corepressors like N-CoR, this silencing C terminus may be the second mechanism by which DAX-1 inhibits Ad4BP/SF-1 transactivation. This silencing carboxyl terminus also correlates with naturally occurring AHC mutations. Coexistence of GFP-DAX-1 and YFP-Ad4BP/SF-1 dramatically changed the fluorescence pattern of both proteins from diffuse distributions to the formation of clear dots, with the two fluorescence signals completely overlapping. The FRAP data in this study revealed that the intranuclear mobility of Ad4BP/SF-1 was also affected upon interaction with DAX-1.

Agonist-bound nuclear receptors form nuclear matrix-bound foci and are believed to be capable of undergoing rapid exchange. As an example, E2 treatment leads ER and the cofactor SRC-1 to strongly interact with the nuclear matrix, after which ER is partially immobilized, possibly representing interaction with more immobilized components of the nuclear structure. Ligand-bound ER and SRC-1 are still capable of rapid recovery within seconds of photobleaching. In the case of an ER antagonist, ER is extremely immobilized with no appreciable photobleaching recovery for several minutes at least, and this immobilization provides a new explanation for the inhibitory effects of the ER antagonist (21). The orphan receptor Ad4BP/SF-1 was also found to be quite mobile within the nucleus, with a mean recovery $t_{1/2}$ of around 0.8 sec after photobleaching. DAX-1 had a very different effect on Ad4BP/SF-1 with respect to the intranuclear mobility. Coexpression of DAX-1 resulted in clearly reduced mobility of Ad4BP/SF-1. These data, together with the result that Ad4BP/SF-1 and DAX-1 undergo the formation of colocalized dots upon interacting with each other, suggest that Ad4BP/SF-1 might be tightly bound to some special structure in the nuclear matrix upon binding with DAX-1. DAX-1 might work as an anchor protein mediating the sharp immobilization of Ad4BP/SF-1 in the nuclear matrix structure. Protein-protein interaction might affect the intracellular mobility of some steroid receptor and thereby contribute to their biological activity.

However, forskolin treatment enabled Ad4BP/SF-1 to recover from the transactivation suppression induced by DAX-1 as evidenced by the luciferase assay and by the fact that the complete overlapping of Ad4BP/SF-1 and DAX-1 signals was partially separated upon PKA activation. This was further supported by the FRAP data showing that the DAX-1-reduced mobility of Ad4BP/SF-1 was rescued by the activation of PKA. These data collectively suggest that activation of PKA may weaken the interaction between DAX-1 and Ad4BP/SF-1 and may disassemble DAX-1 from Ad4BP/SF-1, thus leading to the recovery of Ad4BP/SF-1 transcriptional activity. A previous study also demonstrated that the presence or absence of DAX-1 could not change the SF-1-SF-1-responsive element EMSA result (31). This means that, although DAX-1 can bind directly to SF-1, when SF-1 is activated and binds to the promoters of target genes, it is SF-1 alone, not in combination with DAX-1, that binds to the DNA, *i.e.* DAX-1 must now be stripped from binding with SF-1.

In the Ad4BP/SF-1 amino acid sequence, two regions were determined to be important for the interaction with DAX-1 (11). One is termed the R domain, which is between amino acids 437 and 447, and the other is residue 226 to 230 (ELILQ) of Ad4BP/SF-1. It is intriguing that the interaction between Ad4BP/SF-1 and the coactivator SRC-1 also requires the same residues (ELILQ), leading to the logical deduction that Ad4BP/SF-1-DAX-1 binding and Ad4BP/SF-1-coactivator binding may be mutually competitive, *i.e.* the Ad4BP/SF-1-interacting coactivator-repressor balance may determine the transactivation ability of Ad4BP/SF-1. Based on our present study, activation of the PKA signal pathway leads to the recruitment of the GCN5/TRRAP coactivator complex, and also to the disassembly of the inhibitory DAX-1, both of which may finally direct the coactivator-repressor balance to favoring the activation of Ad4BP/SF-1.

Collectively, activation of PKA can assemble Ad4BP/SF-1 to an active state, as manifested by foci formation, and this process is accompanied by the recruitment of coactivators GCN5/TRRAP, which might represent a newly identified cofactor complex for Ad4BP/SF-1. Direct interaction between Ad4BP/SF-1 and the repressor DAX-1 was visualized as completely overlapping fluorescent dots, and DAX-1 sharply immobilized Ad4BP/SF-1 upon binding. Activation of PKA was able to disrupt or weaken the interaction between DAX-1 and Ad4BP/SF-1 and therefore rescue the Ad4BP/SF-1 transactivation capability. In conclusion, activation of PKA may reintegrate the protein-protein interactions between Ad4BP/SF-1 and its coactivators and repressor, which finally decide the Ad4BP/SF-1 transactivation capability.

MATERIALS AND METHODS

Cell Culture

The human ovarian granulosa-like tumor cell line KGN was originally established by our group and expresses a high level of aromatase activity that is PKA dependent (47); the cells also highly express Ad4BP/SF-1 (48). The cells were maintained in DMEM/Nutrient Mixture F-12, Life Technologies, Inc., Gaithersburg, MD) supplemented with 10% fetal bovine serum, 10 U/liter penicillin, and 10 μg/ml streptomycin in an atmosphere of 5% CO_2 at 37 C. NIH-3T3 and CV1 cells were obtained from American Type Culture Collection (Manassas, VA) and maintained in DMEM supplemented with 10% fetal bovine serum, 10 U/liter penicillin and 10 μg/ml streptomycin in 75-cm^2 flasks at 37 C in 5% CO_2.

Plasmid Constructions

A full-length human Ad4BP/SF-1 cDNA was cloned from a human spleen cDNA library (BD Bioscience CLONTECH, Palo Alto, CA) by PCR using primers based on the human Ad4BP/SF-1 cDNA sequence (GenBank accession no. NM 004959.2). The PCR was performed using an Advantage cDNA PCR kit (BD Bioscience CLONTECH) and an automated thermo-cycler (Whatman Biometra, Gottingen, Germany) with the appropriate program. The PCR product was first subcloned into the pGEM-T-Easy vector (Promega Corp., Madison, WI) and sequenced to validate its structure using an ABI PRIM 377 DNA sequencer (PE Applied Biosystems, Foster City, CA). Finally, Ad4BP/SF-1 cDNA was subcloned into the expression vector pcDNA3.1 (+) (Invitrogen, San Diego, CA) at the *Not*I and *Xba*I restriction sites to produce pcDNA 3.1-Ad4BP/SF-1.

A mutant human Ad4BP/SF-1 cDNA construct containing the G35E mutation found in the patient (8) was made using a QuikChange site-directed mutagenesis kit (Stratagene, La Jolla, CA). Full-length cDNAs of wild-type and mutant Ad4BP/SF-1 were then subcloned into the *Sac*II sites of both pEGFP-C1 and pEYFP-C1 (CLONTECH Laboratories, Inc.), downstream of the humanized GFP or YFP sequence. The boundary regions between GFP (or YFP) and the human Ad4BP/SF-1 cDNAs were sequenced to validate that the Ad4BP/SF-1 cDNAs were placed in the reading frame of GFP or YFP. A human full-length DAX-1 expression vector pRc/RSV-DAX-1 was prepared as previously described (49). The expression plasmids for GFP-DAX-1 chimeras were constructed by inserting the full-length DAX-1 cDNA into the *Hin*dIII and *Xba*I sites of pEGFP-C3 (CLONTECH Laboratories, Inc.). Expression vectors pcDNA3-GCN5 and pcDNA3-TRRAP were constructed previously (30). To make GFP-GCN5, the full-length GCN5 cDNA was inserted into the *Eco*RI-*Xba*I sites of pEGFP-C2, downstream of the fluorescence protein. Chimeras for TRRAP-GFP, TRRAP-YFP, and TRRAP-CFP were prepared by inserting the full-length TRRAP cDNA into the *Eco*RI site of pEGFP-N1, pEYFP-N1, and pECFP-N1, respectively, in which TRRAP was fused to the N terminus of the fluorescent proteins. The firefly luciferase reporter vector pGL3-ArPII construct containing a 1.0-kb human cytochrome P450 CYP19 ArPII was described previously (50).

Relative Luciferase Reporter Assay

On the first day, 1.5×10^5 cells per well in 1 ml growth medium were seeded into 12-well plates. On the second day, 0.8 μg of PGL3-ArPII, 2.0 ng of phRL-CMV, and a total amount of 0.15μg of expression vectors for human Ad4BP/SF-1, chimerical fluorescent protein-Ad4BP/SF-1, or Ad4BP/SF-1 plus other plasmids such as DAX-1, GCN5, TRRAP, or their fluorescent protein chimerical plasmids were transiently cotransfected to each well using the Superfect transfection reagent (QIAGEN, Valencia, CA) following the manufacturer's protocol. For coexpression studies, the total amount of plasmid DNA added to each well was equalized by the addition of empty vector. On the third day, the culture medium was replaced with fresh medium in the presence or absence of 10^{-6} mol/liter forskolin (Sigma-Aldrich Corp., St. Louis, MO). On the fourth day, the cells were lysed in 100 μl/well passive lysis buffer, and the luciferase assay was performed in accordance with the protocol of the Dual-Luciferase Reporter Assay System, using a Lumat LB 9507 luminometer (Berthold Technologies, Bad Wildbad, Germany). The firefly luciferase activity produced by PGL3-ArPII in identically treated triplicate samples was normalized for the renilla luciferase activity produced by phRL-CMV. The data shown are representative of at least three independent experiments.

Living-Cell Laser Confocal Fluorescence Microscopy and FRAP

On the first day, 3×10^5 KGN cells were seeded in 35-mm glass-based dishes (IWAKI, Asahi Techno Glass, Chiba, Japan). On the second day, a total amount of 0.5 μg/dish of various test chimera plasmids was transfected into cells using Superfect. Four hours post transfection, the culture medium was replaced with fresh medium in the presence or absence of 10^{-6} mol/liter forskolin. After overnight incubation (12 h), cells were observed using an LSM 510 META microscope (Carl Zeiss) equipped with a Plan-Apochromat ×100 1.4 oil objective.

Transient transfected proteins will potentially cause artifacts from overexpression. Transient transfection also results in a clear cell-to-cell difference of XFP-fusion protein expression level within the same cell population. To roughly overcome these complications, a reference system relating the overexpression level of GFP-X to the endogenous X expression level was established by a quantitative immunofluorescence staining. As a brief example, GFP-DAX-1 is at first transfected to KGN cells, which on the next day was subjected to immunostaining by an anti-DAX-1 antibody and an Alexa Fluor 546-sec antibody. The Alexa Fluor 546 intensity between transfected cells (bearing GFP signal; Alexa Fluor 546 intensity represents both GFP-DAX-1 and endogenous DAX-1), and nontransfected cells (Alexa Fluor 546 intensity represents only endogenous DAX-1) were compared quantitatively and a reference of respective GFP intensity was established. Only cells expressing less than 10-fold [which is usually believed to be near physiological (21)] of endogenous protein level were selected for imaging.

For single fluorescent protein imaging, GFP or YFP fluorescence was excited by the 488-nm or 514-nm laser line, respectively, from an air-cooled fiber-coupled argon laser. For simultaneous imaging of GFP and YFP, a 488-nm laser line was used for excitation, and detection spectrum range was from 491–576 nm. For simultaneous imaging of GFP, YFP, and CFP, a 458-nm laser line was used for excitation, and detection spectrum range was set from 458–587 nm. Raw imagines obtained in a λ-mode were subjected to the META Unmixing procedure to de-mix GFP, YFP, and CFP signals. The reference spectrums for each XFPs were made by imaging cells solely expressing each respective XFP. For GFP, YFP, CFP trilocalization imagining, all three references spectrums were applied for META Unmixing, whereas only GFP and YFP reference spectrums were applied to unmix the GFP and YFP bilocalization images.

Matching the expression levels of proteins being cotransfected is essential to observing a reasonable subcellular interaction. For cotransfection, the amount of each XFP-fusion plasmid was equivalent on a molar basis. During simultaneous multiimaging, cells that express a similar intensity of each fluorescence protein were selected for further study. Parameters such as the laser power, laser line, dichroic beam splitter to separate excitation and emission, scanning speed *etc.*, were all kept fixed during observation of the same group of experimental cells. Colocalization analysis was carried out by LSM software (version 3.0). Line scan analysis was also performed by the software. Fluorescent intensity numerals of each line scan were exported to MS Excel, the mean ± SD as well as HI values of intensity value for segment of interest were calculated. MS Excel also constructed the line scan fluorescent intensity fluctuation graphs of the representative cells. All images obtained represent the average of eight sequentially obtained images. LSM images were exported as TIF files, and final figures were generated using Adobe Illustrator and Adobe Photoshop (Adobe Systems, Inc., San Jose, CA).

Fluorescence recovery after photobleaching (FRAP) analysis were also carried out by the LSM 510 META confocal microscope. A single Z section was imaged before and at time intervals after a 2-sec bleach. The bleach was carried